Electronic Supplementary Material (ESI) for Physical Chemistry Chemical Physics.

Table of content

1. Equipment and synthesis

1.1. Equipment

All reagents and solvents were reagent grade and were purchased from Penta, Aldrich, Apollo and TCI and used as received. The starting 4-substituted phenylboronic pinacol esters/acid **7**–**9**/**10** and activated methylene compounds **11**–**16** are commercially available. Compounds **1a**–**4a** were already published in the literature.[1,2,3,4] Solvents were evaporated on Heidolph Hei-VAP value rotary evaporator. Column chromatography was carried out with silica gel 60 (particle size 0.040–0.063 mm, 230–400 mesh; Merck) and commercially available solvents. Thin-layer chromatography (TLC) was conducted on aluminium sheets coated with silica gel 60 F_{254}, obtained from Merck, with visualization by a UV lamp (254 or 366 nm). ^{1}H, ^{13}C and ^{19}F NMR spectra were recorded on a Bruker AVANCE III 500 spectrometer (500 MHz, 125 MHz or 470 MHz, respectively). Chemical shifts are reported in ppm relative to the signal of Me_4Si (0.00 ppm) and C_6F_6 (164.90 ppm). The residual solvent signal was used as an internal reference ($CDCl_3$ 7.25 and 77.23 ppm). Apparent resonance multiplicities are described as s (singlet), d (doublet), dd (doublet of doublet), and m (multiplet). The coupling constants, *J*, are reported in Hertz (Hz). High-resolution MALDI mass spectroscopy data were collected on an LTQ Orbitrap XL equipped with nitrogen UV laser (337 nm, 60 Hz). The LTQ Orbitrap instrument was operated in positive-ion mode over a normal mass range (*m/z* 100–2000) with resolution 100 000 at *m/z* = 400. 2-[(2*E*)-3-(4-*Tert*-butylphenyl)-2-methylprop-2-enylidene]malononitrile (DCTB) was used as a matrix. Mass spectra were averaged over the whole MS record for all measured samples. Thermal properties were determined by differential scanning calorimetry DSC with a Mettler-Toledo STARe System DSC 2/700 equipped with FRS 6 ceramic sensor and cooling system HUBER TC100-MT RC 23. Thermal behaviour of the target compounds was measured in aluminous crucibles sealed with a punctured lid under N_2 inert atmosphere (65 ml×min^{-1}). DSC curves were recorded with a scan rate of 5 °C/min within the range 25–600 °C. The electrochemical behaviour was investigated in ACN containing 0.1 M Bu_4NPF_6 in a three-electrode cell by cyclic voltammetry (CV). The recorded peak potentials are given vs. SSCE. Absorption and fluorescence spectra were measured on a Duetta™ HORIBA spectrophotometer in THF, ACN, $CHCl_3$ and toluene at 25 °C. Compounds were excited at their absorption maxima (band of the lowest energy) to record the emission spectra. Fluorescence quantum yield (±10%) was determined relative to that of anthracene or perylene in cyclohexane (ϕ_f = 0.39 resp. 0. 94). The Time Correlated Single Photon Counting Method (TCSPC) has been employed to detect the fluorescence dynamics in the ps to ns timescale (Picoquant Fluotime 200). For this reason, a 400 nm diode laser was used with a pulse duration of 60 ps. The overall instrument's response function (IRF) was ~ 80 ps. Multi-exponential functions were used to fit the experimental data considering the system's IRF. The quality of the fittings was determined via the χ^2 parameter, which should be less than 1.1. The 2PA measurements were performed using the Two-Photon Excited Fluorescence Method (TPEF).[5] A 80 fs Ti:Sapphire mode locked laser with wavelengths ranging from 730-870 nm was used. Determination of the 2PA cross sections has been made using the equation:

[1] S. Q. Fu, M. Z. Zhu, B. Xue and P. N. Liu, *Macromolec.* 2022, **55**, 8784.
[2] C. Hongbiao, X. Siqi, L. Huaming and Y. Mei, *CN106905526*.
[3] S. K. Sachan and G. Anantharaman, *Inorg. Chem.* 2021, **60**, 9238.
[4] F. Shibahara, E. Yamaguchi and T. Murai, *J. Org. Chem.* 2011, **76**, 2680.
[5] N.S. Makarov, M. Drobizhev, A. Rebane, *Optics Express* 2008, **16**, 4029.

$$\delta_{TPA}^{S} = \frac{k_r F_S \Phi_s^F n_r C_r P_r}{k_s F_r \Phi_s^F n_s C_s P_s} \delta_{TPA}^{r}$$

with a solution of Rhodamine 6G in MeOH as a reference sample (r). *k* is the collection factor of the set-up, considering the wavelength response of the detector and optics, *F* is the detected two-photon excited fluorescence intensity, Φ^F is the fluorescence quantum yield, *n* is the refractive index of the samples, *c* is the concentration and *P* is the excitation power. The target molecules (s) were examined in toluene and THF with concentration of 2×10^{-5} M. The quadratic law dependence of the emitted fluorescence vs. the excitation power was followed in all cases. The experimental error on the reported cross sections is 15%.

1.2. Synthesis of 1-methyl-2,4,5-tribromoimidazole (**1**)

Commercial 2,4,5-tribromoimidazole (8 g, 26 mmol) was suspended in 130 ml of water in a 250 ml round bottom flask. $NaHCO_3$ (3.6 g, 43 mmol) and NaOH (1.7 g, 43 mmol) were added followed by a slow addition of dimethylsulfate (4.3 ml, 26 mmol). The mixture was heated at 65 °C for 1 h and cooled to 25 °C. The precipitate was filtered off, washed with water and air-dried affording 3.6 g (43 %) of **1** as a white solid. M.p. = 93-95 °C; ^{1}H NMR (500 MHz, $CDCl_3$, 25 °C): δ = 3.62 (s, 3H) ppm; ^{13}C NMR (125 MHz, $CDCl_3$, 25 °C): δ = 118.58, 116.45, 105.82, 35.04; EI/MS (70 eV), *m/z* (%): 318 (M^+,100), 320 (100), 239 (75), 316 (38), 322 (34). EI/MS (70 eV), *m/z* (%): 318 (M^+,100), 320 (100), 239 (75), 316 (38), 322 (34).

1.3. Suzuki-Miyaura cross-coupling reactions towards **1a**–**4a**

In a Schlenk flask, 1-methyl-2,4,5-tribromoimidazole **1** (318 mg, 1.0 mmol) and boronic esters or acid **7**–**10** (4.0 mmol) were dissolved in a mixture of 1,4-dioxane/H_2O (25 mL, 4:1). Argon was bubbled through the solution for 10 min, whereupon $Pd(PPh_3)_4$ (84 mg, 0.07 mmol) and K_2CO_3 (690 mg, 5.0 mmol) were added and the resulting reaction mixture was stirred at 110 °C for 72 h. The reaction mixture was diluted with water (100 mL) and extracted with CH_2Cl_2 (3 × 50 mL). The combined organic extracts were washed with water, dried over anhydrous Na_2SO_4, the solvents were evaporated *in vacuo* and the crude product was purified by column chromatography.

1.3.1 4,4',4''-(1-Methyl-1*H*-imidazole-2,4,5-triyl)tribenzaldehyde (**1a**)

The title compound was prepared from **1** (318 mg, 1.0 mmol) and 4-(4,4,5,5-tetramethyl-1,3,2-dioxaborolan-2-yl)benzaldehyde **7** (928 mg, 4 mmol) following the general method. The crude product was purified by column chromatography (SiO_2, CH_2Cl_2/EtAc, 5:1). Yield: 312 mg (79 %); yellowish solid; R_f = 0.50 (SiO_2; CH_2Cl_2/EtAc, 5:1); ^{1}H NMR (500 MHz, $CDCl_3$, 25°C): δ = 10.10 (s, 1H), 10.08 (s, 1H), 9.92 (s, 1H), 8.02-7.87 (m, 6H), 7.73 (d, *J* = 8 Hz, 2H), 7.65 (d, *J* = 8 Hz, 2H), 7.60 (d, *J* = 8 Hz, 2H), 3.61 (s, 3H) ppm; ^{13}C NMR (100 MHz, $CDCl_3$, 25°C): δ = 191.57, 191.65, 191.46, 136.81, 136.74, 135.15, 131.92, 131.47, 130.69, 130.14, 130.07, 129.83, 127.68, 34.09 ppm; HR-FT-MALDI-MS (DCTB): m/z calcd. for $C_{25}H_{18}N_2O_3$ $[M]^+$ 394.13174; found: 394.13069.

1.3.2 4,4',4''-(1-Methyl-1*H*-imidazole-2,4,5-triyl)tribenzonitrile (**2a**)

The title compound was prepared from **1** (318 mg, 1.0 mmol) and 4-(4,4,5,5-tetramethyl-1,3,2-dioxaborolan-2-yl)benzonitrile **8** (916 mg, 4 mmol) following the general method for the Suzuki–Miyaura reaction. The crude product was purified by repeated column chromatography (SiO_2, CH_2Cl_2/EtAc, 5:1). Yield: 98 mg (25 %); white solid; R_f = 0.25 (SiO_2; CH_2Cl_2/EtAc, 5:1); ^{1}H NMR (500 MHz, $CDCl_3$, 25 °C): δ =7.89 (d, *J* = 8 Hz, 2H), 7.83-7.80 (m, 4H), 7.56-7.51 (m, 6H), 3.58 (s, 3H) ppm; ^{13}C NMR (125 MHz, $CDCl_3$, 25 °C): *δ* = 147.57, 137.95, 137.86, 134.54, 134.06, 133.42, 132.80, 132.52, 131.50, 131.28, 129.64, 127.57, 119.08, 118.44, 118.18, 113.66, 113.29, 110.81, 33.97 ppm; HR-FT-MALDI-MS (DCTB): *m/z* calcd. for $C_{25}H_{15}N_5$ $[M+H]^+$ 386.14053; found: 386.13929.

1.3.3 Trimethyl 4,4',4''-(1-methyl-1*H*-imidazole-2,4,5-triyl)tribenzoate (**3a**)

The title compound was prepared from **1** (318 mg, 1.0 mmol) and methyl 4-(4,4,5,5-tetramethyl-1,3,2-dioxaborolan-2-yl)benzoate **9** (1.048 g, 4.0 mmol) following the general method for the Suzuki–Miyaura reaction. The crude product was purified by column chromatography (SiO_2, CH_2Cl_2/EtAc, 5:1). Yield: 256 mg (53 %); white solid; R_f = 0.60 (SiO_2; CH_2Cl_2/EtAc, 5:1); ^{1}H NMR (500 MHz, $CDCl_3$, 25 °C): *δ* = 8.15-8.12 (m, 4H), 7.87-7.83 (m, 4H), 7.54 (d, *J* = 8 Hz, 2H), 7.46 (d, *J* = 8 Hz, 2H), 3.94 (s, 1H), 3.93 (s, 1H), 3.85 (s, 1H), 3.54 (s, 3H) ppm; ^{13}C NMR (125 MHz, $CDCl_3$, 25 °C): *δ* = 167.13, 166.70, 166.61, 147.86, 134.92, 131.56, 130.88, 130.73, 130.62, 130.10, 129.82, 129.11, 128.50, 127.01, 52.59, 52.52, 52.18, 33.86 ppm; HR-FT-MALDI-MS (DCTB): *m/z* calcd. for $C_{28}H_{24}N_2O_6$ $[M]^+$ 484.16344; found: 484.16190.

1.3.4 1-Methyl-2,4,5-tris(4-(trifluoromethyl)phenyl)-1*H*-imidazole (**4a**)

The title compound was prepared from **1** (318 mg, 1.0 mmol) and (4-(trifluoromethyl)phenyl)boronic acid **10** (760 mg, 4.0 mmol) following the general method for the Suzuki–Miyaura reaction. The crude product was purified by column chromatography (SiO_2, CH_2Cl_2). Yield: 298 mg (58 %); white solid; R_f = 0.80 (SiO_2; CH_2Cl_2); ^{1}H NMR (500 MHz, $CDCl_3$, 25 °C): *δ* = 7.87 (d, *J* = 8 Hz, 2H), 7.77 (d, *J* = 8 Hz, 2H), 7.58 (d, *J* = 8 Hz, 2H), 7.54 (d, *J* = 8 Hz, 2H), 7.48 (d, *J* = 8 Hz, 2H), 3.55 (s, 3H) ppm; ^{13}C NMR (125 MHz, $CDCl_3$, 25 °C): *δ* = 147.64, 137.95, 137.58, 134.26, 133.94, 131.83, 131.68, 131.57, 131.51, 131.42, 131.32, 131.16, 131.09, 131.05, 130.90, 130.79, 129.70, 129.50, 129.33, 129.27, 129.08, 128.82, 128.56, 127.70, 127.54, 127.49, 127.46, 127.36, 127.25, 127.00, 126.60, 126.57, 126.54, 126.51, 126.21, 126.00, 125.97, 125.94, 125.91, 125.71, 125.57, 125.54, 125.51, 125.48, 125.20, 125.11, 123.37, 123.03, 125.95, 121.21, 120.87, 120.78, 33.69 ppm; HR-FT-MALDI-MS (DCTB): *m/z* calcd. for $C_{25}H_{15}F_9N_2$ $[M]^+$ 514.10915; found: 514.10814.

1.4. Knoevenagel condensation towards **1b**–**6b**

Tricarbaldehyde **1a** (80 mg, 0.2 mmol) and corresponding activated methylene compound **11**–**16** (0.8 mmol) were dissolved in CH_2Cl_2 (10 mL) and Al_2O_3 (306 mg, 3 mmol, Brockmann II–III) was added. The reaction mixture was stirred at 25 °C for 48 h, filtered and the solvent was evaporated in vacuo. The crude product was purified by column chromatography.

1.4.1. 2,2',2''-(((1-Methyl-1*H*-imidazole-2,4,5-triyl)tris(benzene-4,1-diyl))tris(methaneylylidene))trimalononitrile (**1b**)

The title compound was prepared from **1a** (80 mg, 0.2 mmol) and malononitrile **11** (53 mg, 0.8 mmol) following the general method for the Knoevenagel condensation. The crude product was purified by column chromatography (SiO_2, CH_2Cl_2/EtAc, 5:1). Yield: 60 mg (55 %); red-orange solid; R_f = 0.40 (SiO_2; CH_2Cl_2/EtAc, 5:1); ^{1}H NMR (500 MHz, $CDCl_3$, 25 °C): δ = 8.09-8.06 (m, 4H), 7.98 (d, J = 8 Hz, 2H), 7.85 (s, 1H), 7.83 (s, 1H), 7.80 (d, J = 8 Hz, 2H), 7.67 (s, 1H), 7.64 (d, J = 8 Hz, 2H), 7.60 (d, J = 8 Hz, 2H), 3.65 (s, 3H) ppm; ^{13}C NMR (125 MHz, $CDCl_3$, 25 °C): δ = 159.08, 158.63, 158.35, 147.94, 140.03, 138.55, 135.75, 135.36, 132.47, 131.82, 131.47, 131.71, 131.48, 131.35, 131.20, 129.77, 127.83, 114.08, 113.59, 113.42, 113.00, 112.60, 112.47, 84.62, 83.97, 81.55, 34.19 ppm; HR-FT-MALDI-MS (DCTB): *m/z* calcd. for $C_{34}H_{18}N_8$ $[M]^+$ 538.16544; found: 538.16497.

1.4.2. Triethyl 3,3',3''-((1-methyl-1*H*-imidazole-2,4,5-triyl)tris(benzene-4,1-diyl))(2*E*,2'*E*,2''*E*)-tris(2-cyanoacrylate (**2b**)

The title compound was prepared from **1a** (80 mg, 0.2 mmol) and ethyl 2-cyanoacetate **12** (90 mg, 0.8 mmol) following the general method for the Knoevenagel condensation. The crude product was purified by column chromatography (SiO_2, CH_2Cl_2/EtAc, 10:1). Yield: 68 mg (50 %); yellow solid; R_f = 0.6 (SiO_2; CH_2Cl_2/EtAc, 10:1); ^{1}H NMR (500 MHz, $CDCl_3$, 25 °C): δ = 8.31 (s, 1H), 8.29 (s, 1H), 8.16 (s, 1H), 8.15-8.13 (m, 4H), 7.93 (d, J = 8 Hz, 2H), 7.88 (d, J = 8 Hz, 2H), 7.63 (d, J = 8 Hz, 2H), 7.56 (d, J = 8 Hz, 2H), 4.43-4.33 (m, 6H), 3.62 (s, 3H), 1.42-1.35 (m, 9H) ppm; ^{13}C NMR (125 MHz, $CDCl_3$, 25 °C): δ = 162.88, 162.42, 162.29, 154.60, 153.94, 153.71, 147.96, 138.40, 134.80, 132.36, 132.24, 132.03, 131.68, 131.51, 131.49, 130.08, 129.59, 127.62, 115.99, 115.59, 115.50, 104.47, 103.96, 101.69, 63.13, 63.07, 62.76, 34.05, 14.31 ppm; HR-FT-MALDI-MS (DCTB): *m/z* calcd. for $C_{40}H_{33}N_5O_6$ $[M]^+$ 679.24308; found: 679.24167.

1.4.3. 2,2',2''-(((1-Methyl-1*H*-imidazole-2,4,5-triyl)tris(benzene-4,1-diyl))tris(methaneylylidene))tris(1*H*-indene-1,3(2*H*)-dione) (**3b**)

The title compound was prepared from **1a** (80 mg, 0.2 mmol) and indan-1,3-dione **13** (117 mg, 0.8 mmol) following the general method for the Knoevenagel condensation. The crude product was purified by column chromatography (SiO_2, CH_2Cl_2/EtAc, 5:1). Yield: 90 mg (58 %); red solid; R_f = 0.35 (SiO_2; CH_2Cl_2/EtAc, 5:1); ^{1}H NMR (500 MHz, $CDCl_3$, 25 °C): δ = 8.63 (d, J = 8 Hz, 4H), 8.40 (d, J = 8 Hz, 2H), 8.05-8.03 (m, 4H), 7.98-7.95 (m, 6H), 7.85-7.83 (m, 5H), 7.76 (dd, J = 3 Hz and J = 6 Hz, 2H), 7.73 (d, J = 8 Hz, 2H), 7.61 (d, J = 8 Hz, 2H), 3.68 (s, 3H) ppm; ^{13}C NMR (125 MHz, $CDCl_3$, 25 °C): δ = 190.76, 190.32, 190.20, 189.45, 189.31, 189.28, 148.46, 147.01, 145.88, 145.63, 142.83, 142.82, 142.73, 140.40, 140.38, 140.25, 139.34, 138.82, 135.85, 135.78, 135.70, 135.63, 135.44, 135.23, 135.10, 135.02, 134.91, 134.69, 134.45, 133.98, 133.78, 132.95, 132.02, 131.15, 130.39. 130.06, 129.25, 128.53, 127.42, 123.74, 123.73, 123.69, 123.67, 123.43, 123.41, 34.26 ppm; HR-FT-MALDI-MS (DCTB): *m/z* calcd. for $C_{52}H_{30}N_2O_6$ $[M+H]^+$ 779.21823; found: 779.21476.

1.4.4. (5*Z*,5'*Z*,5''*Z*)-5,5',5''-(((1-Methyl-1*H*-imidazole-2,4,5-triyl)tris(benzene-4,1-diyl))tris(methaneylylidene))tris(3-ethyl-2-thioxothiazolidin-4-one) (**4b**)

The title compound was prepared from **1a** (80 mg, 0.2 mmol) and 3-ethylrhodanine **14** (128 mg, 0.8 mmol) following the general method for the Knoevenagel condensation. The crude product was purified by column chromatography (SiO_2, CH_2Cl_2/EtAc, 10:1). Yield: 112 mg (68 %); orange solid; R_f = 0.85 (SiO_2; CH_2Cl_2/EtAc, 10:1); ^{1}H NMR (500 MHz, $CDCl_3$, 25 °C): δ = 7.89 (d, *J* = 8 Hz, 2H), 7.76 (d, *J* = 8 Hz, 2H), 7.65-7.61 (m, 7H), 7.53 (d, *J* = 8 Hz, 2H), 7.36 (d, *J* = 8 Hz, 2H), 4.23-4.14 (m, 6H), 3.61 (s, 3H), 1.31-1.24 (m, 9H) ppm; ^{13}C NMR (125 MHz, $CDCl_3$, 25 °C): δ = 193.22, 192.84, 192.62, 167.83, 167.72, 167.71, 148.07, 138.39, 136.70, 134.28, 134.10, 132.95, 132.48, 132.20, 131.95, 131.86, 131.66, 131.57, 131.53, 131.14, 131.07, 129.75, 127.82, 124.84, 124.49, 122.49, 40.14, 40.10, 39.97, 34.04, 12.49, 12.47 ppm; HR-FT-MALDI-MS (DCTB): *m/z* calcd. for $C_{40}H_{33}N_5O_3S_6$ $[M]^+$ 823.09076; found: 823.08925.

1.4.5. (2*E*,2'*E*,2''*E*)-3,3',3''-((1-Methyl-1*H*-imidazole-2,4,5-triyl)tris(benzene-4,1-diyl))tris(2-(phenylsulfonyl)acrylonitrile) (**5b**)

The title compound was prepared from **1a** (80 mg, 0.2 mmol) and 2-(phenylsulfonyl)acetonitrile **15** (145 mg, 0.8 mmol) following the general method for the Knoevenagel condensation. The crude product was purified by column chromatography (SiO_2, CH_2Cl_2/EtAc, 10:1). Yield: 123 mg (70 %); orange solid; R_f = 0.8 (SiO_2; CH_2Cl_2/EtAc, 10:1); ^{1}H NMR (500 MHz, $CDCl_3$, 25 °C): δ = 8.27 (s, 1H), 8.26 (s, 1H), 8.12 (s, 1H), 8.06-8.03 (m, 7H), 7.97 (d, *J* = 8 Hz, 2H), 7.91 (d, *J* = 8 Hz, 2H), 7.77 (d, *J* = 8 Hz, 2H), 7.72-7.56 (m, 12H), 7.52 (d, *J* = 8 Hz, 2H), 3.68 (s, 3H); ^{13}C NMR (125 MHz, $CDCl_3$, 25°C): δ = 150.99, 150.24, 149.93, 147.94, 139.70, 138.42, 138.15, 137.72, 137.63, 135.36, 135.04, 134.97, 134.69, 132.37, 132.01, 131.62, 131.59, 131.46, 131.07, 130.75, 129.95, 129.91, 129.79, 129.70, 128.95, 128.92, 128.78, 128.72, 127.79, 116.33, 115.76, 113.55, 113.49, 113.19, 113.10, 34.11; HR-FT-MALDI-MS (DCTB): *m/z* calcd. for $C_{49}H_{33}N_5O_6S_3$ $[M]^+$ 883.15930; found: 883.15794.

1.4.6. (2*E*,2'*E*,2''*E*)-3,3',3''-((1-Methyl-1*H*-imidazole-2,4,5-triyl)tris(benzene-4,1-diyl))tris(2-((4-fluorophenyl)sulfonyl) acrylonitrile) (**6b**)

The title compound was prepared from **1a** (80 mg, 0.2 mmol) and 2-((4-fluorophenyl)sulfonyl)acetonitrile **16** (159 mg, 0.8 mmol) following the general method for the Knoevenagel condensation. The crude product was purified by column chromatography (SiO_2, CH_2Cl_2/EtAc, 10:1). Yield: 130 mg (69 %); light orange solid; R_f = 0.6 (SiO_2; CH_2Cl_2/EtAc, 10:1); ^{1}H NMR (500 MHz, $CDCl_3$, 25 °C): δ = 8.27 (s, 1H), 8.25 (s, 1H), 8.11 (s, 1H), 8.07-8.05 (m, 8H), 8.01-7.98 (m, 2H), 7.92 (d, *J* = 8 Hz, 2H), 7.79 (d, *J* = 8 Hz, 2H), 7.59 (d, *J* = 8 Hz, 2H), 7.53 (d, *J* = 8 Hz, 2H), 7.32-7.24 (m, 6H), 3.59 (s, 3H); ^{13}C NMR (125 MHz, $CDCl_3$, 25 °C): δ = 167.76, 167.73, 167.54, 165.71, 165.67, 165.49, 151.07, 150.36, 150.05, 148.01, 139.91, 138.48, 135.52, 135.18, 134.14, 134.12, 133.72, 133.69, 133.62, 133.59, 132.50, 132.10, 132.04, 132.00, 131.96, 131.81, 131.72, 131.68, 131.56, 131.00, 130.67, 129.77, 128.70, 127.86, 117.58, 117.53, 117.39, 117.35, 117.20, 116.11, 115.54, 113.58, 113.26, 113.22, 113.12, 34.21; HR-FT-MALDI-MS (DCTB): *m/z* calcd. for $C_{49}H_{30}F_3N_5O_6S_3$ $[M]^+$ 937.13103; found: 937.12928.

2. NMR spectra

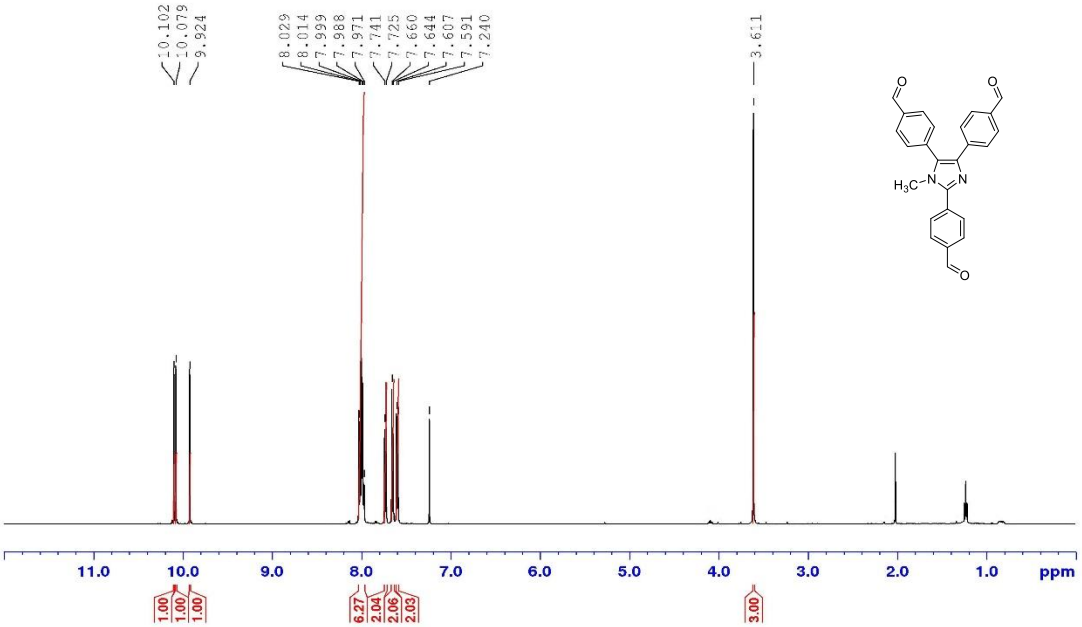

Figure S1. ^{1}H-NMR spectrum of chromophore **1a** (500 MHz, $CDCl_3$, 25 °C).

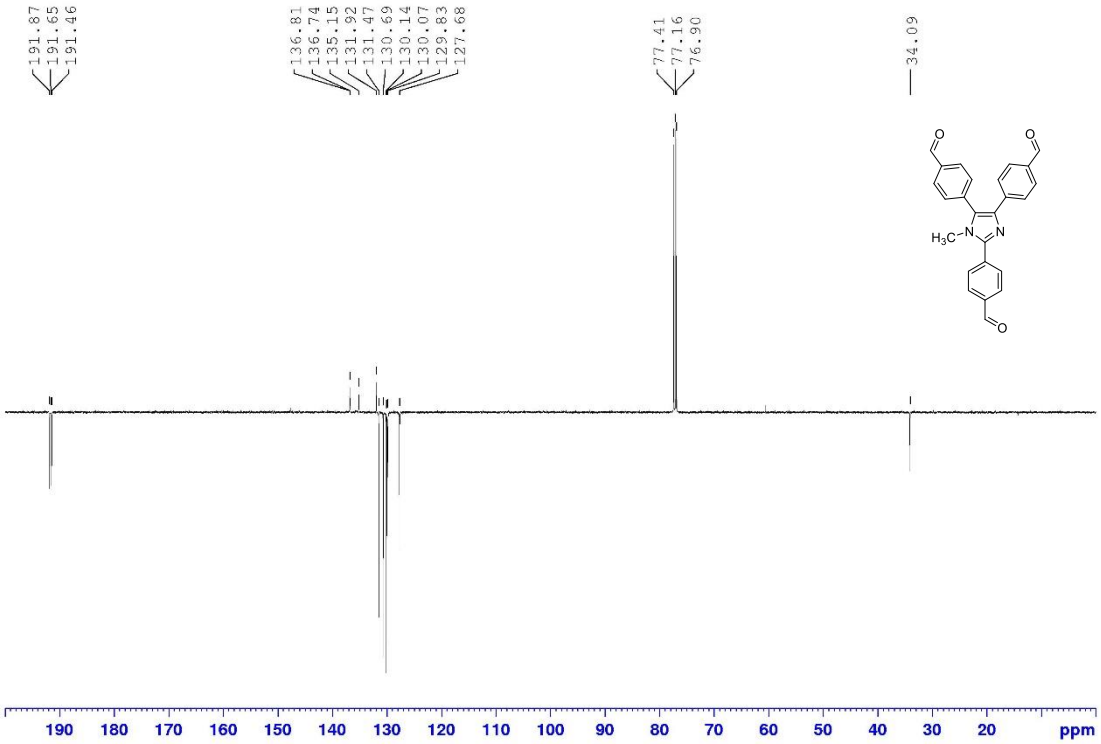

Figure S2. ^{13}C-NMR APT spectrum of chromophore **1a** (125 MHz, $CDCl_3$, 25 °C).

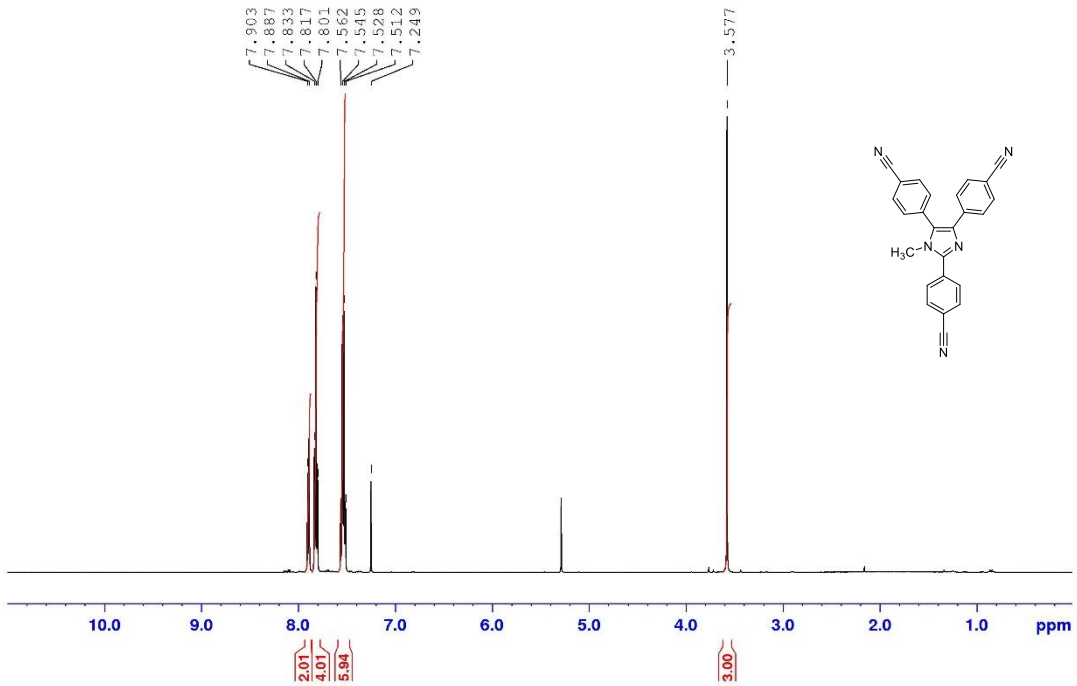

Figure S3. ^{1}H-NMR spectrum of chromophore **2a** (500 MHz, $CDCl_3$, 25 °C).

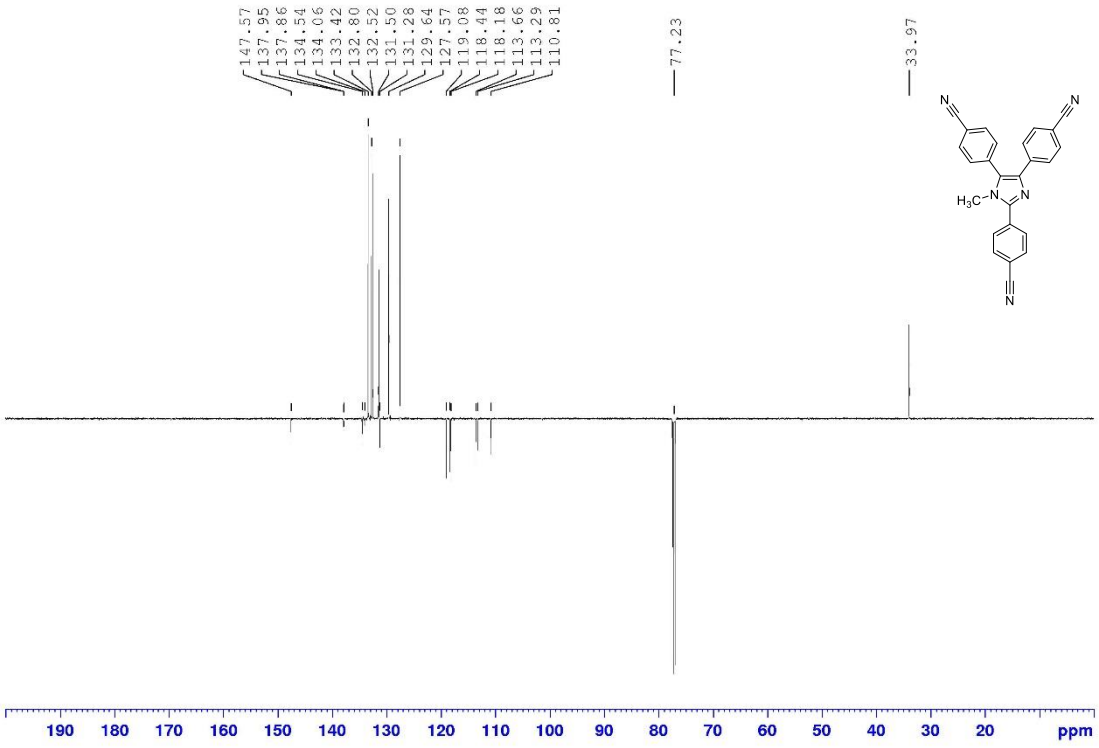

Figure S4. ^{13}C-NMR APT spectrum of chromophore **2a** (125 MHz, $CDCl_3$, 25 °C).

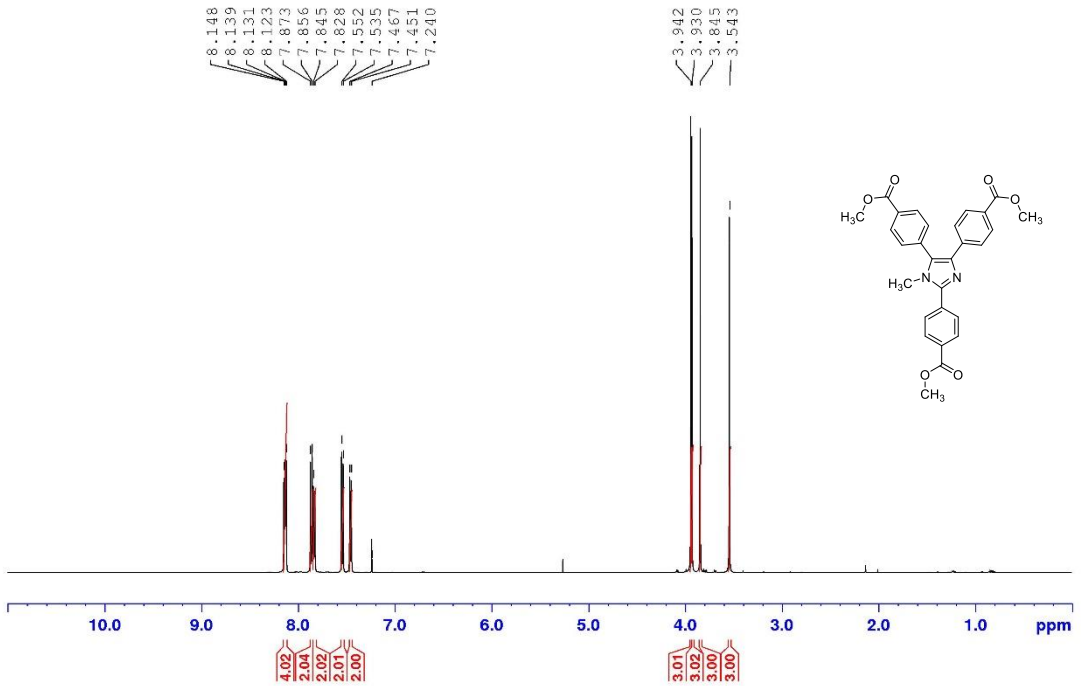

Figure S5. ^{1}H-NMR spectrum of chromophore **3a** (500 MHz, $CDCl_3$, 25 °C).

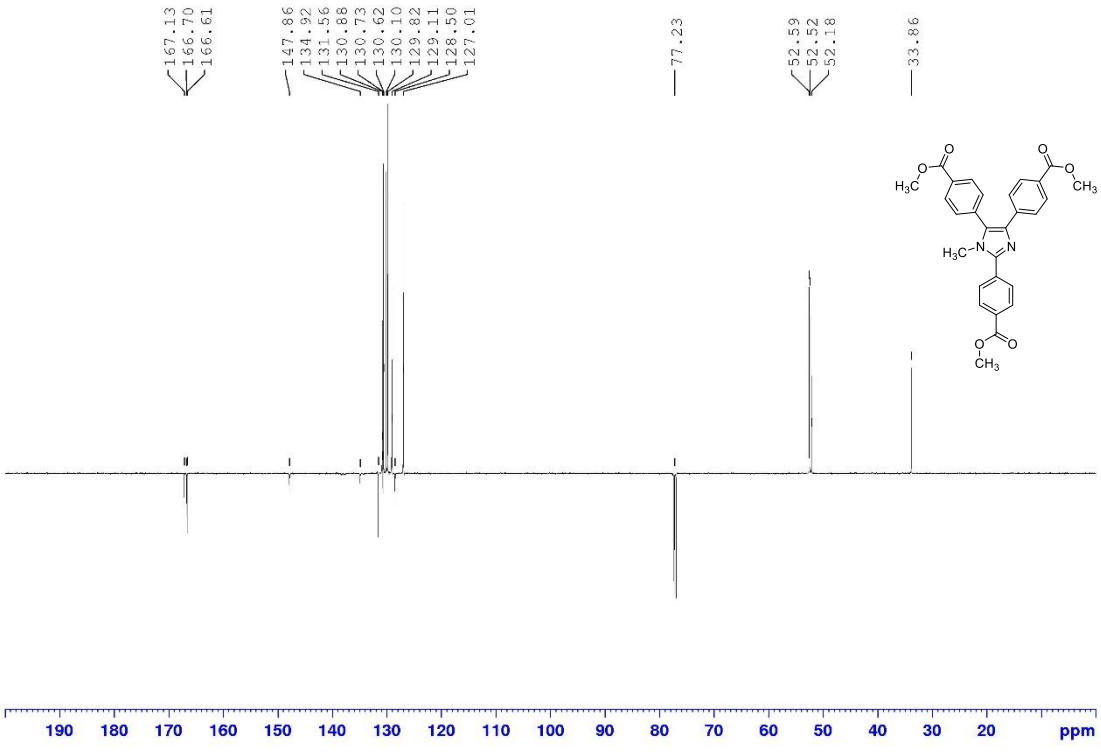

Figure S6. ^{13}C-NMR APT spectrum of chromophore **3a** (125 MHz, $CDCl_3$, 25 °C).

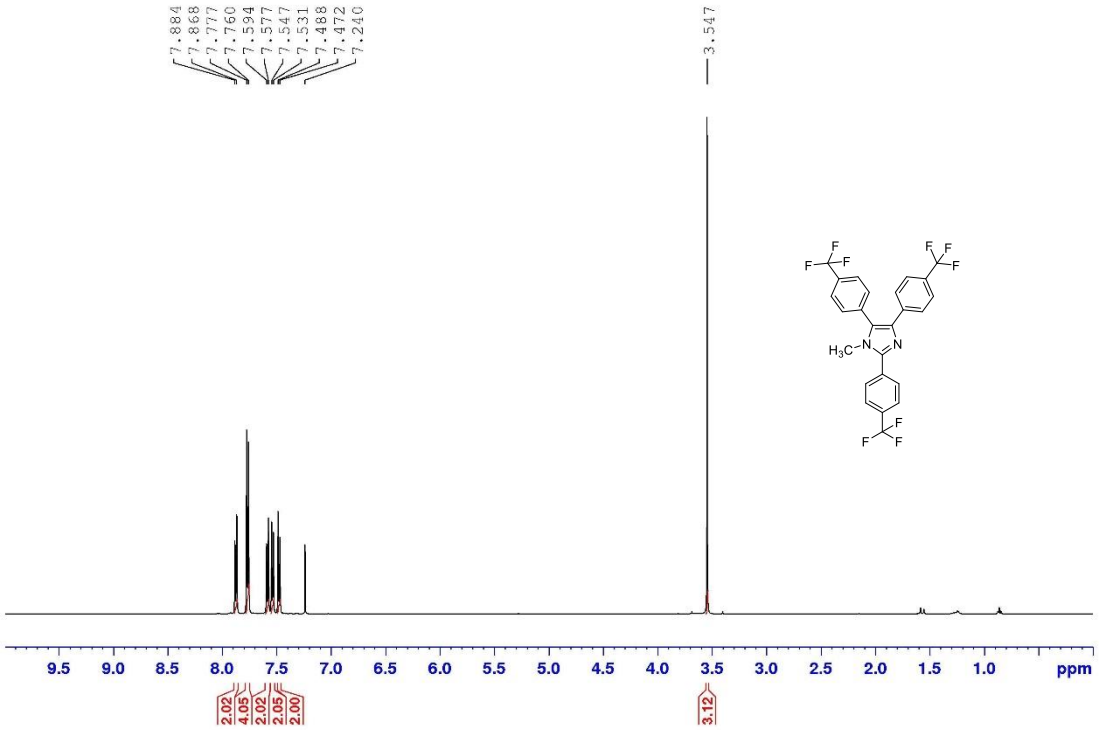

Figure S7. ^{1}H-NMR spectrum of chromophore **4a** (500 MHz, $CDCl_3$, 25 °C).

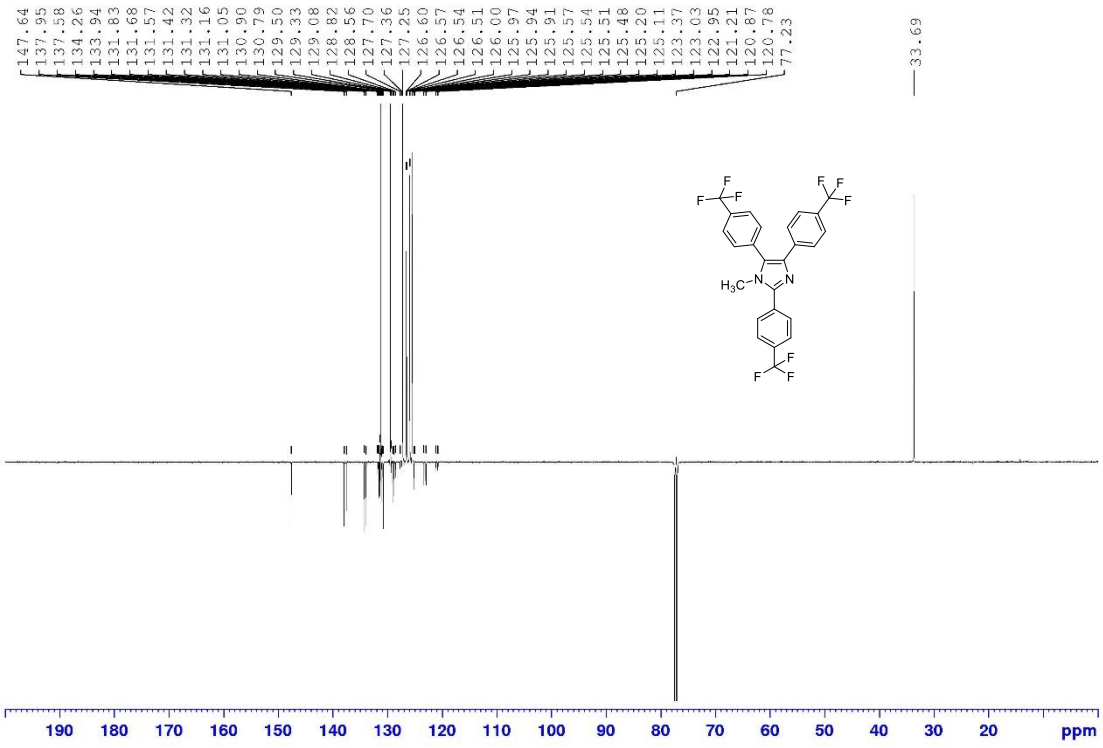

Figure S8. ^{13}C-NMR APT spectrum of chromophore **4a** (125 MHz, $CDCl_3$, 25 °C).

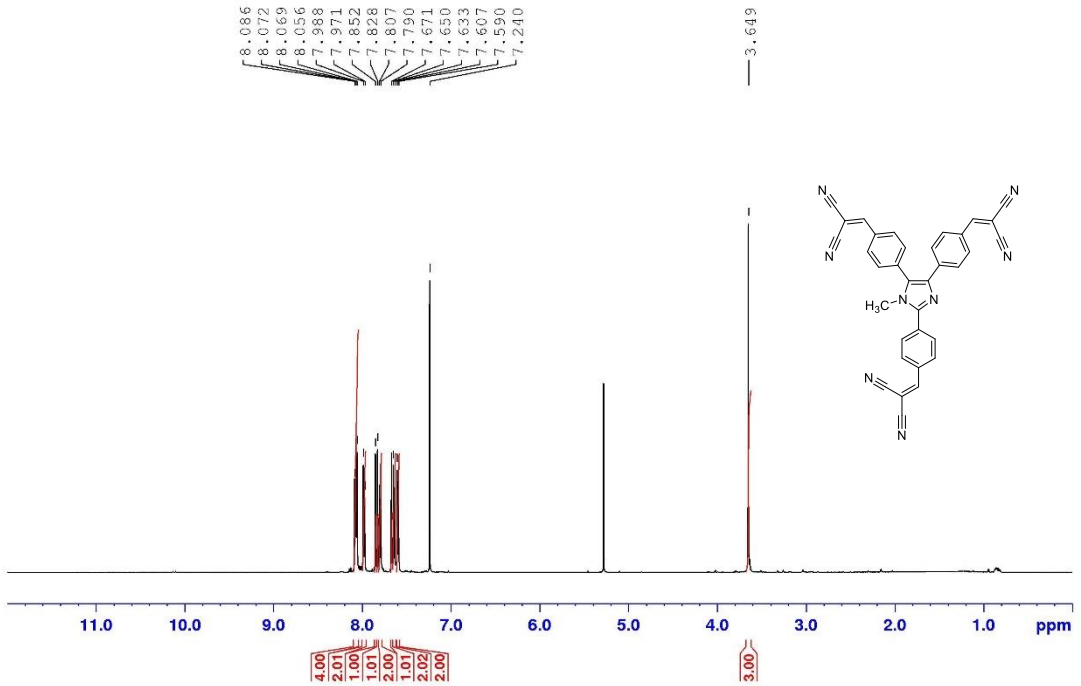

Figure S9. ^{1}H-NMR spectrum of chromophore **1b** (500 MHz, $CDCl_3$, 25 °C).

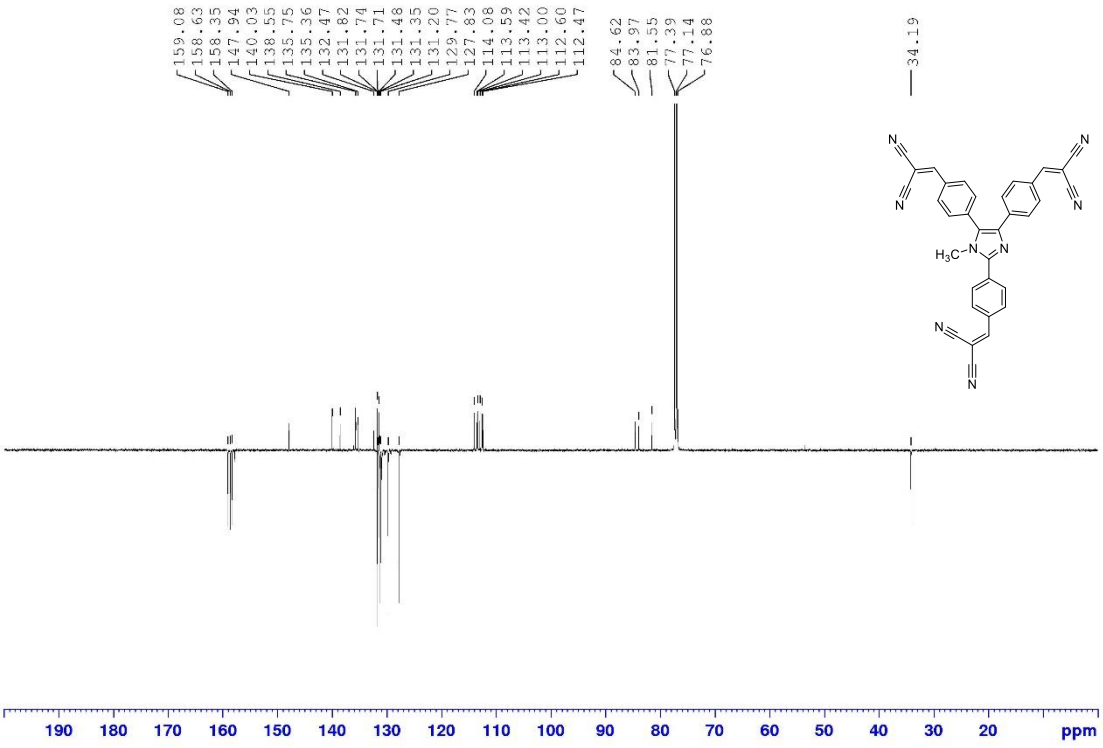

Figure S10. ^{13}C-NMR APT spectrum of chromophore **1b** (125 MHz, $CDCl_3$, 25 °C).

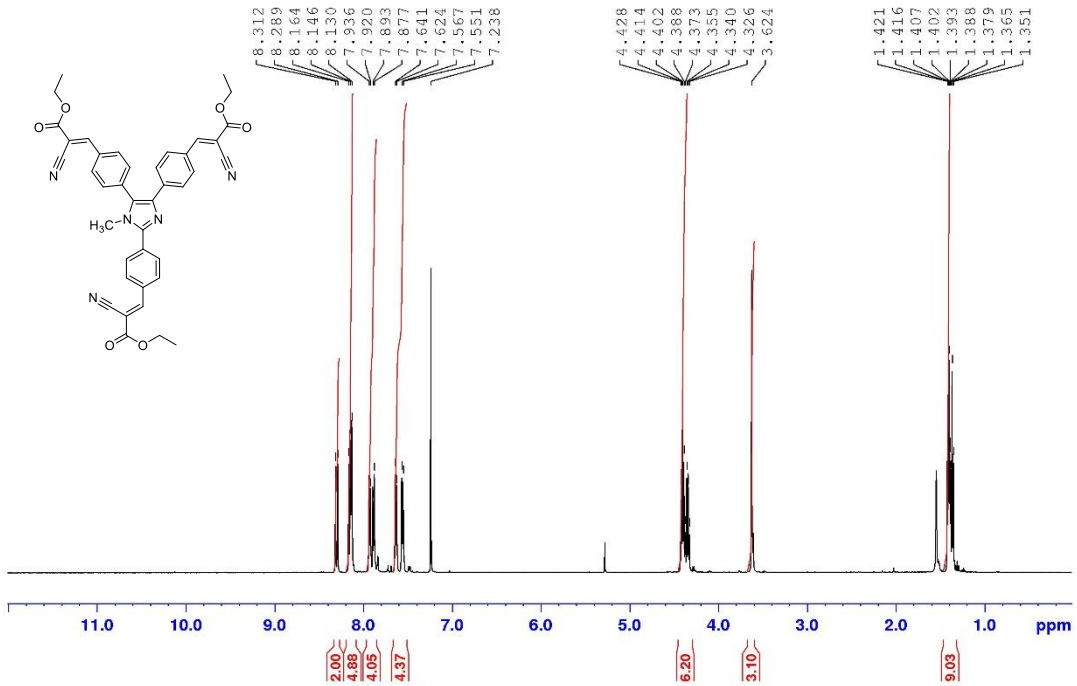

Figure S11. ^{1}H-NMR spectrum of chromophore **2b** (500 MHz, $CDCl_3$, 25 °C).

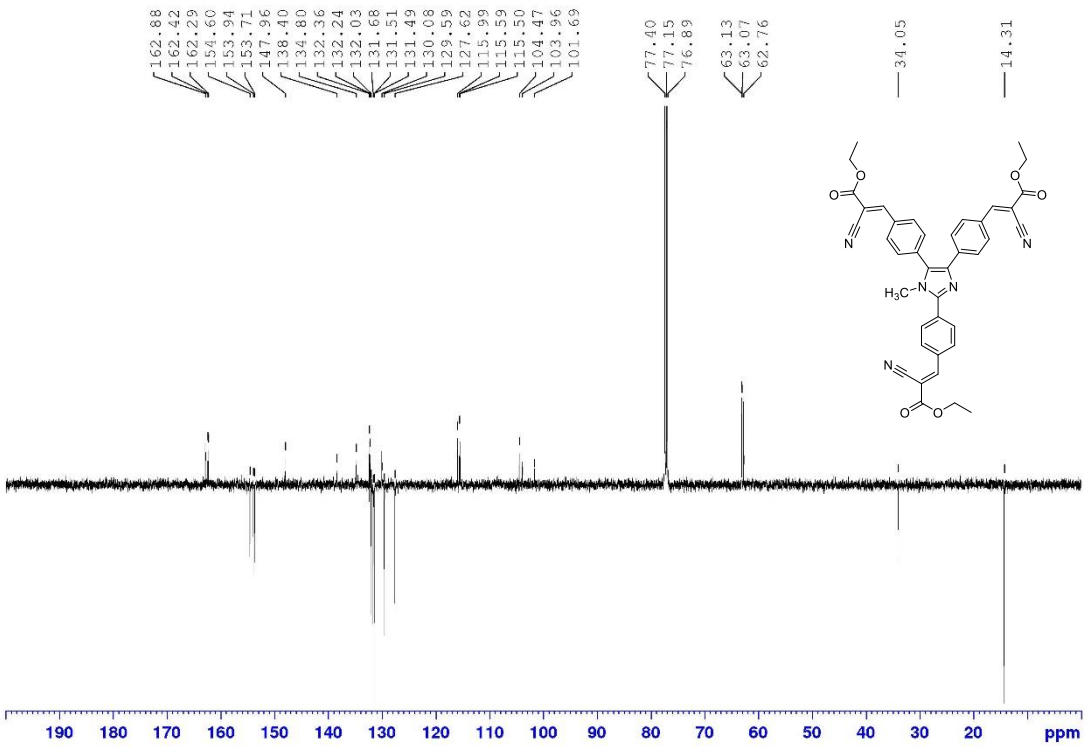

Figure S12. ^{13}C-NMR APT spectrum of chromophore **2b** (125 MHz, $CDCl_3$, 25 °C).

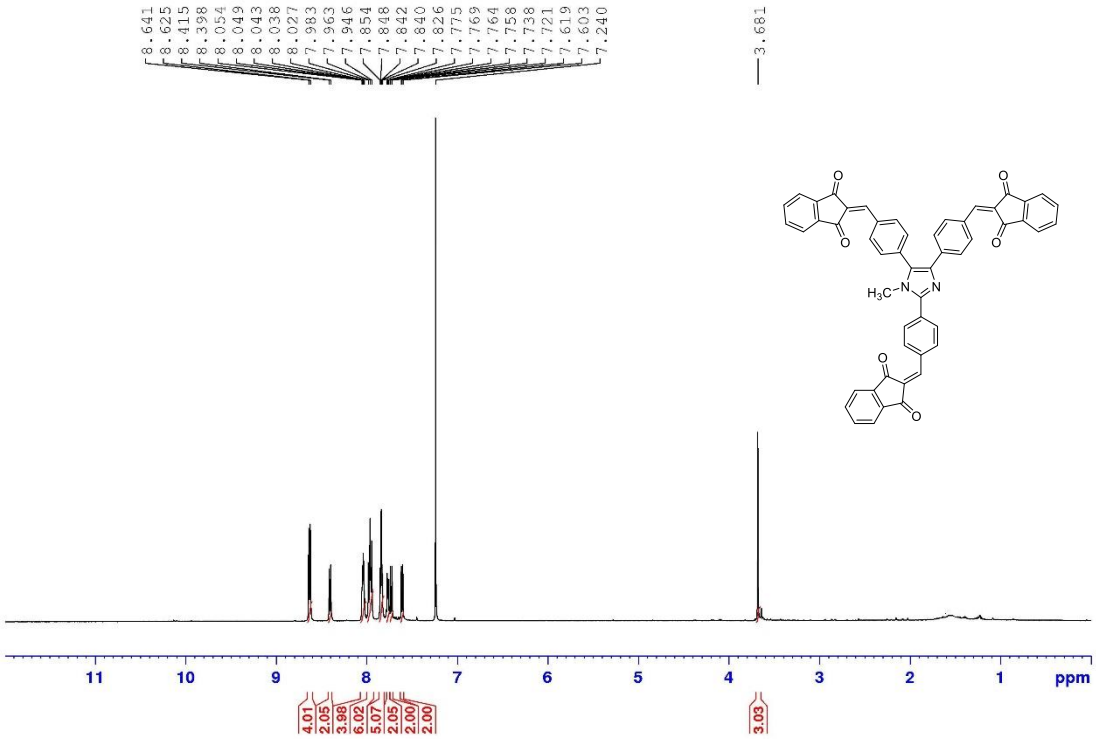

Figure S13. ^{1}H-NMR spectrum of chromophore **3b** (500 MHz, $CDCl_3$, 25 °C).

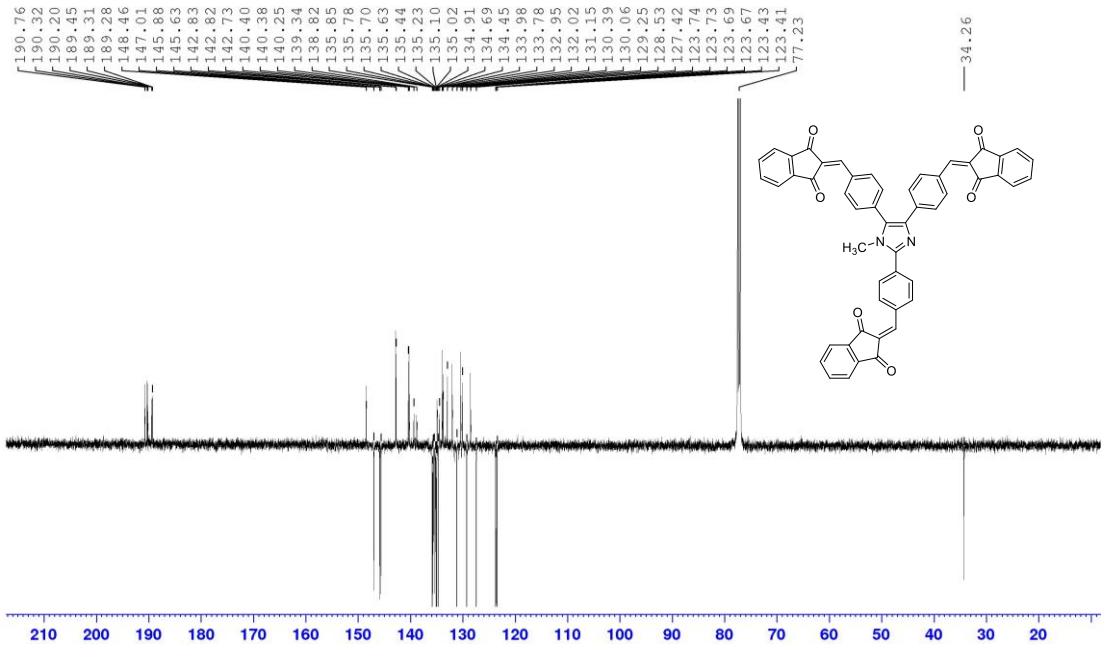

Figure S14. ^{13}C-NMR APT spectrum of chromophore **3b** (125 MHz, $CDCl_3$, 25 °C).

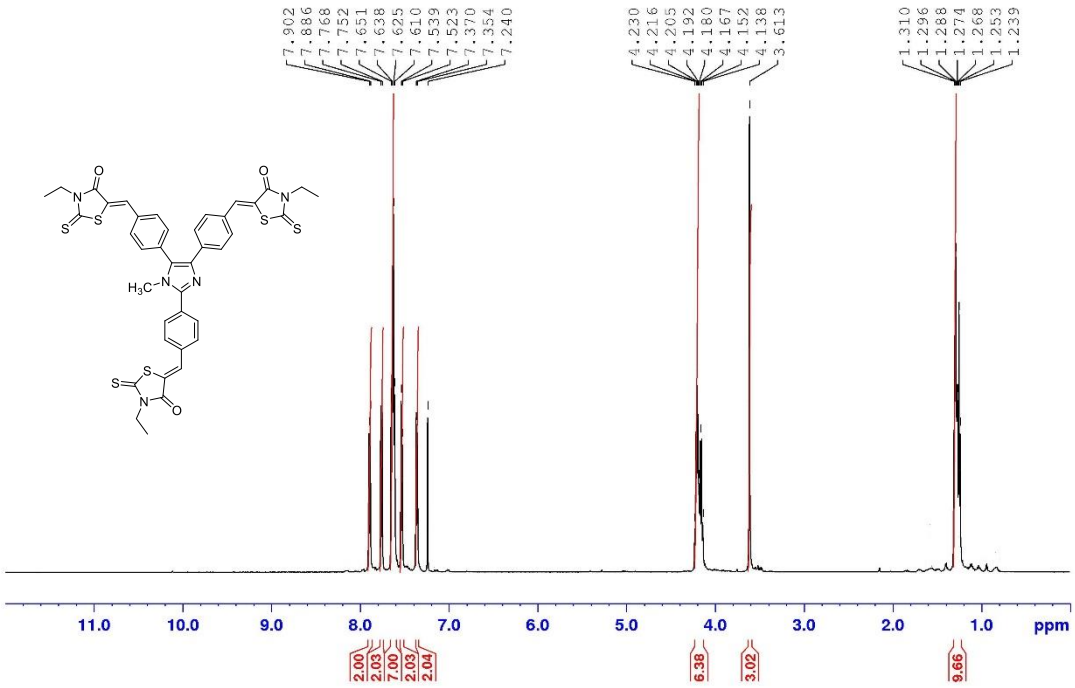

Figure S15. ^{1}H-NMR spectrum of chromophore **4b** (500 MHz, $CDCl_3$, 25 °C).

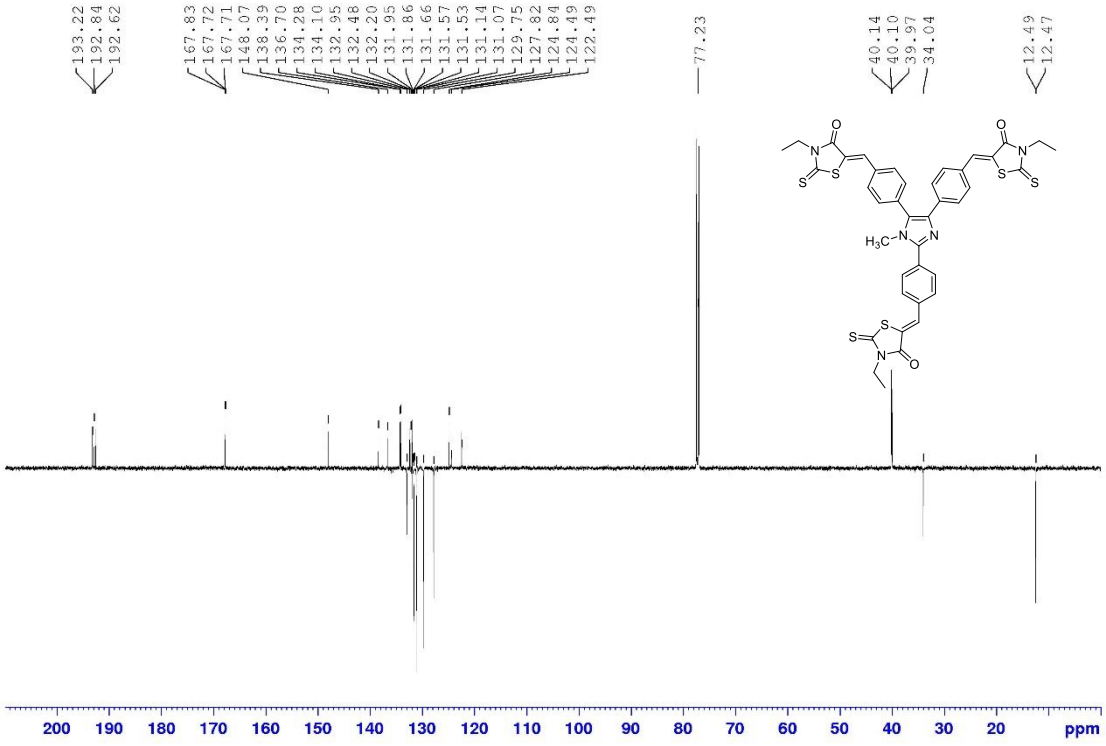

Figure S16. ^{13}C-NMR APT spectrum of chromophore **4b** (125 MHz, $CDCl_3$, 25 °C).

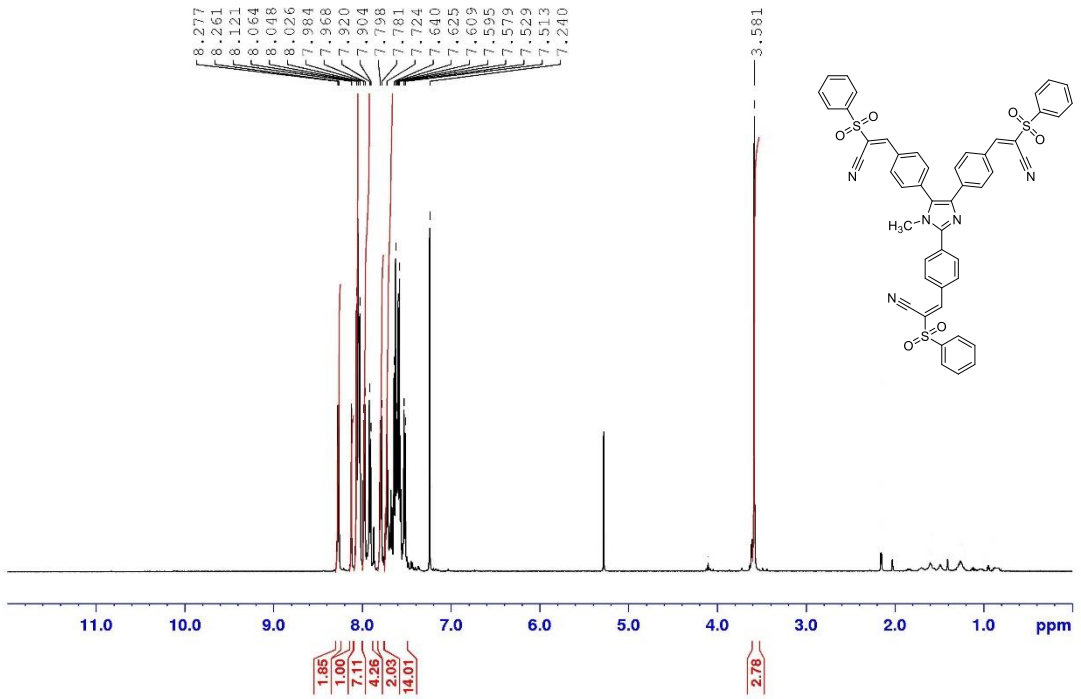

Figure S17. ^{1}H-NMR spectrum of chromophore **5b** (500 MHz, $CDCl_3$, 25 °C).

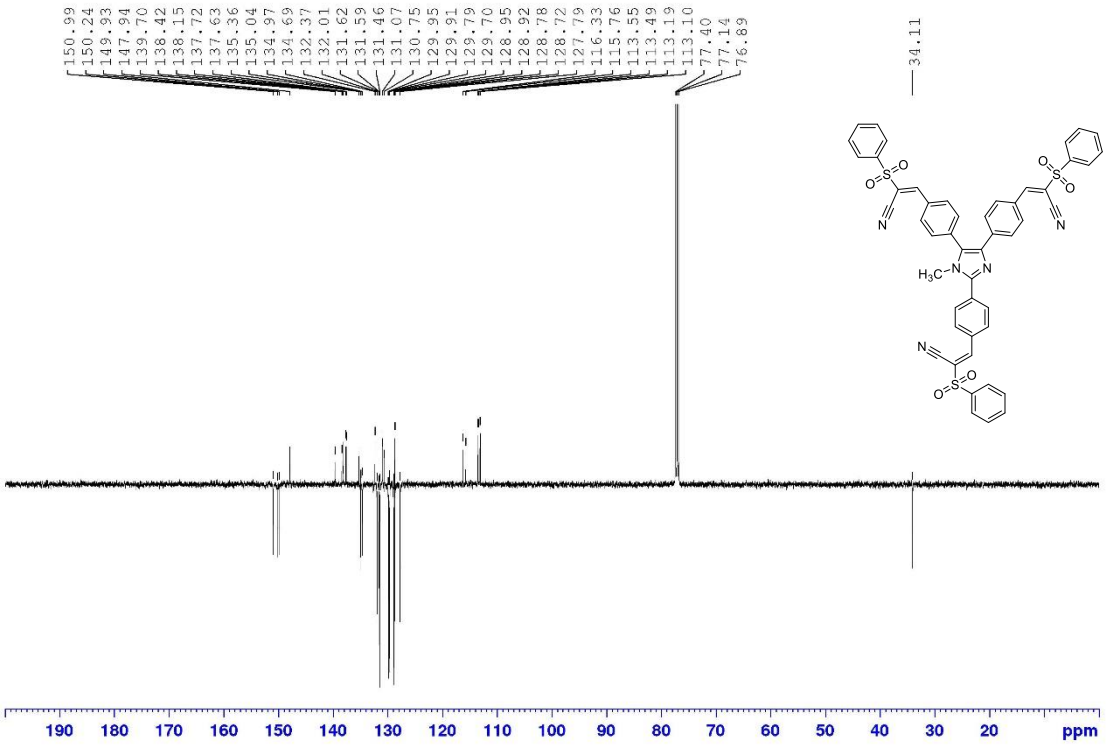

Figure S18. ^{13}C-NMR APT spectrum of chromophore **5b** (125 MHz, $CDCl_3$, 25 °C).

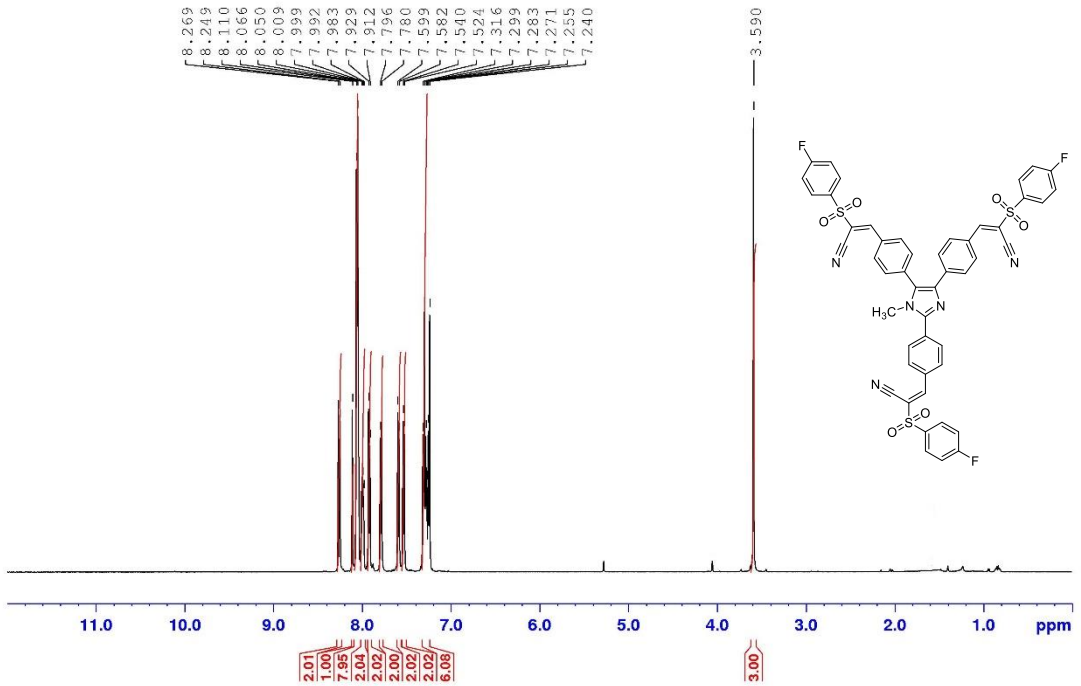

Figure S19. ^{1}H-NMR spectrum of chromophore **6b** (500 MHz, $CDCl_3$, 25 °C).

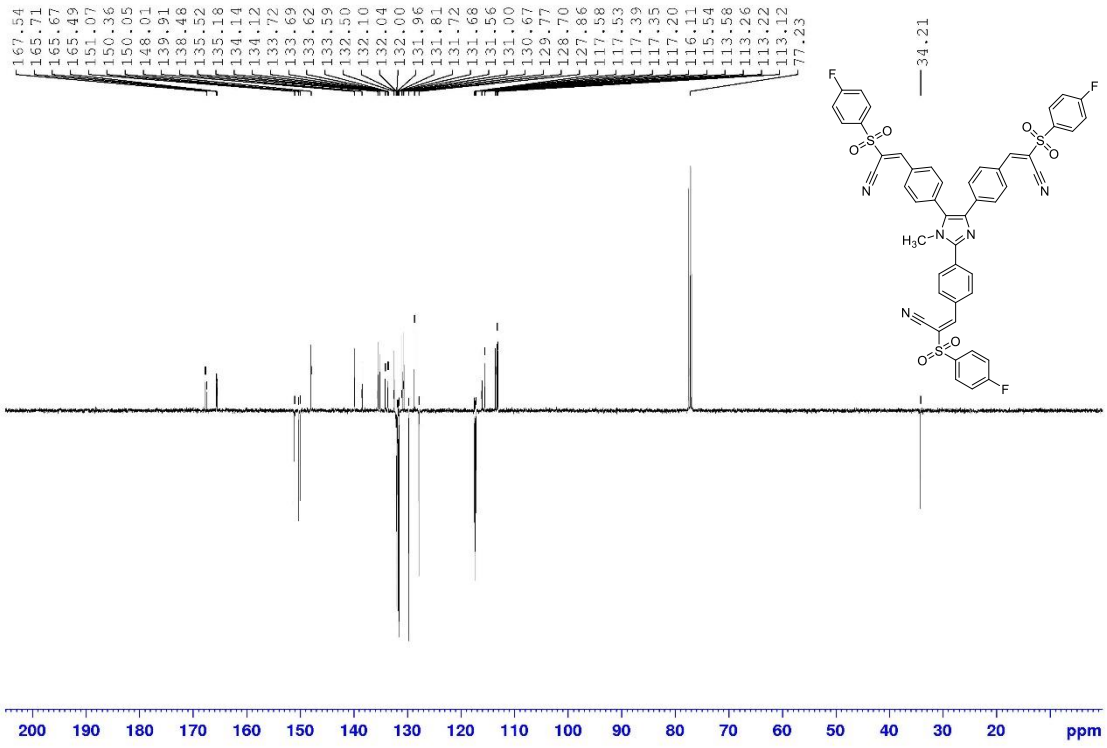

Figure S20. ^{13}C-NMR APT spectrum of chromophore **6b** (125 MHz, $CDCl_3$, 25 °C).

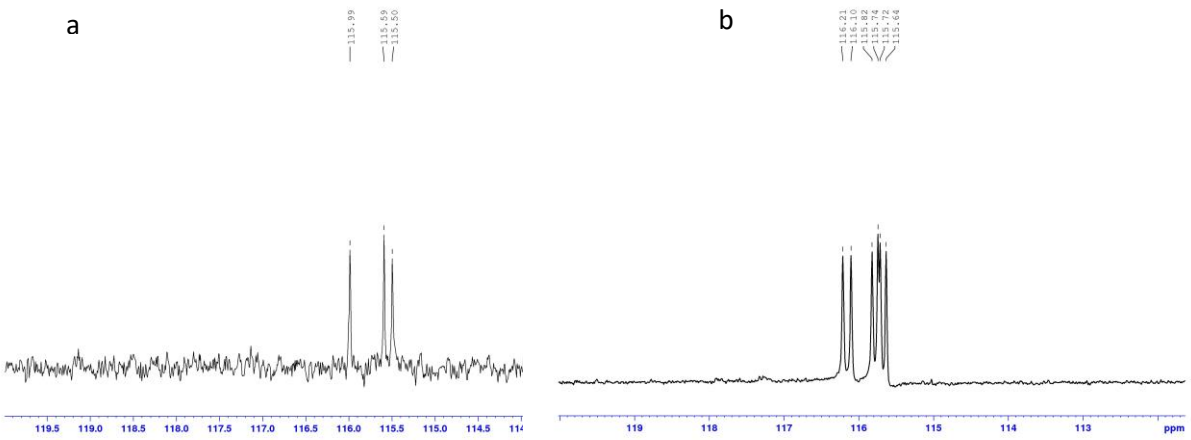

Figure S21. Part of the proton-decoupled (a) and coupled (b) ^{13}C NMR spectrum of chromophore **2b** (125 MHz, $CDCl_3$, 25 °C) used to assign its *E*/*Z*-configuration.

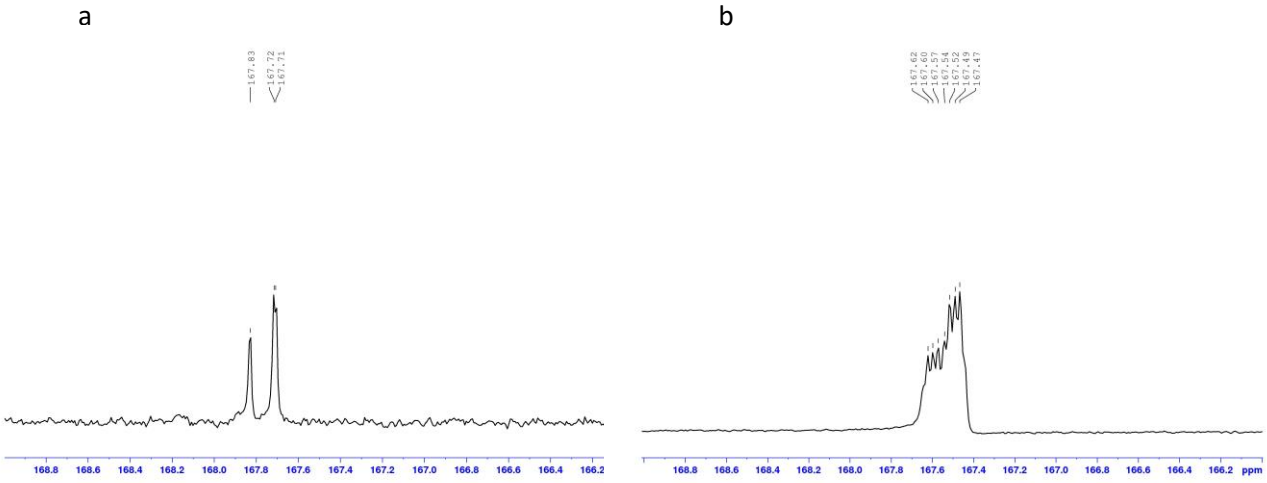

Figure S22. Part of the proton-decoupled (a) and coupled (b) ^{13}C NMR spectrum of chromophore **4b** (125 MHz, $CDCl_3$, 25 °C) used to assign its *E*/*Z*-configuration.

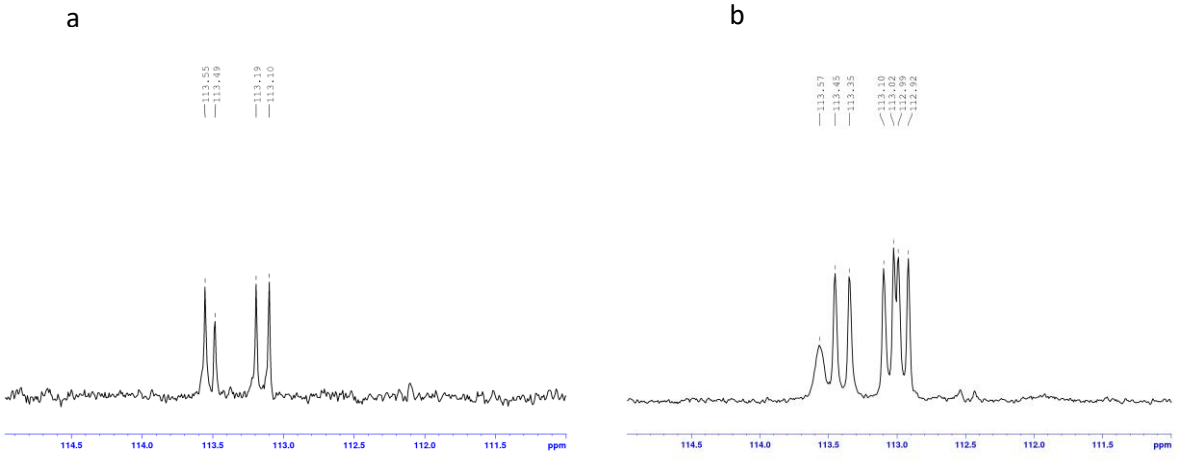

Figure S23. Part of the proton-decoupled (a) and coupled (b) ^{13}C NMR spectrum of chromophore **5b** (125 MHz, $CDCl_3$, 25 °C) used to assign its *E*/*Z*-configuration.

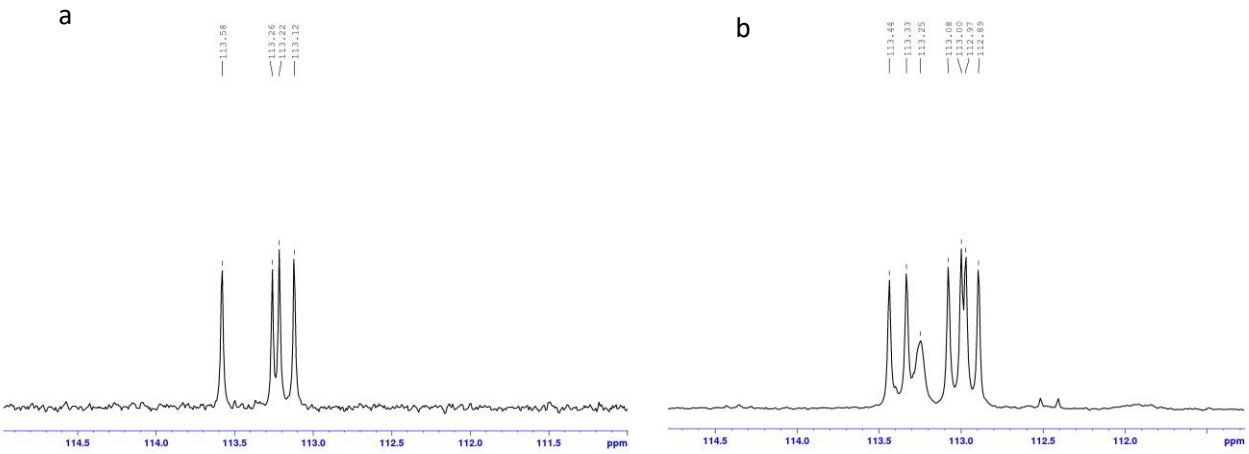

Figure S24. Part of the proton-decoupled (a) and coupled (b) ^{13}C NMR spectrum of chromophore **6b** (125 MHz, $CDCl_3$, 25 °C) used to assign its *E*/*Z*-configuration.

3. X-ray analysis

The X-ray data for colorless crystals of **1a** were obtained at 150K using Oxford Cryostream low-temperature device with a Bruker D8-Venture diffractometer equipped with Mo (Mo/K_α radiation; λ = 0.71073 Å) microfocus X-ray (IμS) source, Photon CMOS detector and Oxford Cryosystems cooling device was used for data collection. Obtained data were treated by XT-version 2014/5 and SHELXL-2017/1 software implemented in APEX3 v2019.1-0 (Bruker AXS) system.[6] $R_{int} = \sum | F_o^2 - F_{o,mean}^2 | / \sum F_o^2$, $S = [\sum(w(F_o^2 - F_c^2)^2)/(N_{diffrs} - N_{params})]^{½}$ for all data, $R(F) = \sum | |F_o| - |F_c| | / \sum |F_o|$ for observed data, $wR(F^2) = [\sum(w(F_o^2 - F_c^2)^2)/(\sum w(F_o^2)^2)]^{½}$ for all data. Crystallographic data for all structural analysis have been deposited with the Cambridge Crystallographic Data Centre, CCDC no. 2331438. Copies of this information may be obtained free of charge from The Director, CCDC, 12 Union Road, Cambridge CB2 1EY, UK (fax: +44-1223-336033; e-mail: deposit@ccdc.cam.ac.uk or www: http://www.ccdc.cam.ac.uk).

The frames were integrated with the Bruker SAINT software package using a narrow-frame algorithm. Data were corrected for absorption effects using the Multi-Scan method (SADABS). The structures were solved and refined using the Bruker SHELXTL Software Package.

Hydrogen atoms were mostly localized on a difference Fourier map, however to ensure uniformity of treatment of crystal, most of the hydrogen atoms were recalculated into idealized positions (riding model) and assigned temperature factors Hiso(H) = 1.2 Ueq (pivot atom) or of 1.5Ueq (methyl). H atoms in methyl moiety and C-H in aromatic rings and aldehydes were placed with C-H distances of 0.97 and 0.93 Å, respectively. In thin crystals of **1a**, the disordered carbonyl group was untreated.

[6] G. M. Sheldrick GM, *Acta Cryst*., 2015, **A71,** 3.

Table S1. Experimental details for **1a**.

Crystal data	
Chemical formula	$C_{25}H_{18}N_2O_3$
M_r	394.41
Crystal system, space group	Monoclinic, $P2_1/n$
Temperature (K)	150
a, b, c (Å)	6.3866 (5), 20.5762 (16), 14.5475 (10)
β (°)	93.315 (3)
V (Å^3)	1908.5 (2)
Z	4
Radiation type	Mo $K\alpha$
μ (mm^{-1})	0.09
Crystal size (mm)	0.59 × 0.24 × 0.04
Data collection	
Diffractometer	Bruker D8 - Venture
Absorption correction	Multi-scan *SADABS2016*/2 - Bruker AXS area detector scaling and absorption correction.[7]
T_{min}, T_{max}	0.607, 0.746
No. of measured, independent and observed [$I > 2\sigma(I)$] reflections	27014, 3663, 3337
R_{int}	0.066
$(\sin \theta/\lambda)_{max}$ (Å^{-1})	0.617
Refinement	
$R[F^2 > 2\sigma(F^2)]$, $wR(F^2)$, S	0.102, 0.218, 1.26
No. of reflections	3663
No. of parameters	272
No. of restraints	237
H-atom treatment	H-atom parameters constrained
$\Delta\rho_{max}$, $\Delta\rho_{min}$ (e Å^{-3})	0.43, −0.35

Computer program: *SHELXL2019*/1 (Sheldrick, 2019).

[7] L. Krause, R. Herbst-Irmer, G. M. Sheldrick and D. Stalke, *J. Appl. Cryst.* 2015, **48**, 3.

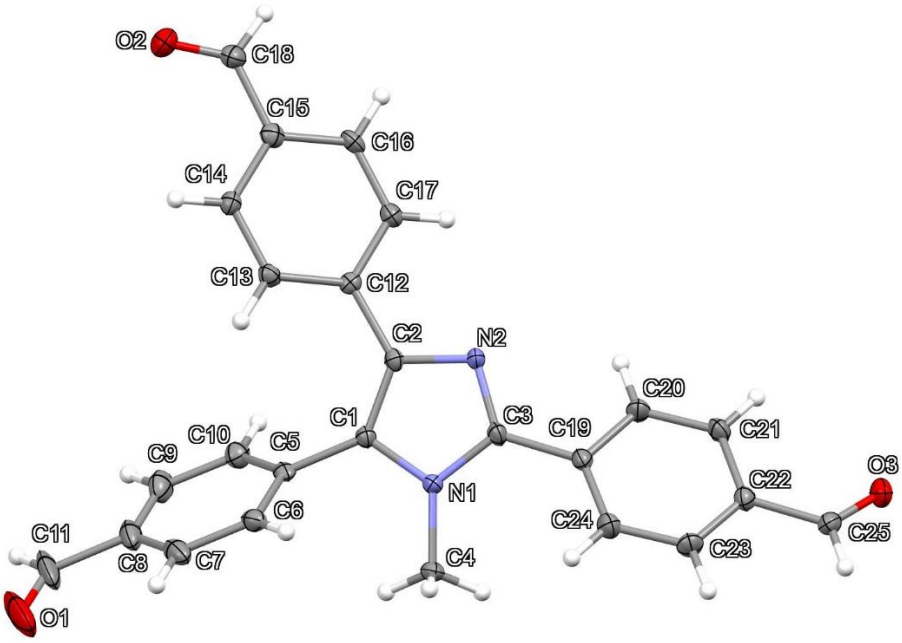

Figure S25. X-ray structure of **1a**, selected intermolecular distances and angles [Å, °]: O1—C11 1.201(8), C1—C2 1.374 (5), C1—N1 1.381(5), C1—C5 1.482(5), N1—C3 1.364(5), N1—C4 1.460(5), C14—C15 1.399(6), O2—C18 1.212(5), C2—N2 1.371(5), C15—C16 1.393 (6), C2—C12 1.478 (5), N2—C3 1.316 (5), C5—C6 1.394(6), C5—C10 1.402 (6), C2—C1—N1 105.2(3), C17—C12—C2 119.2(3), C2—C1—C5 132.6 (4), N1—C1—C5 122.2(3), C3—N1—C1 107.0(3), C3—N1—C4 128.0(3), C1—N1—C4 124.8(3), O1—C11—C8 123.3(6), O2—C18—C15 125.5(4), O3—C25—C22 125.8(4).

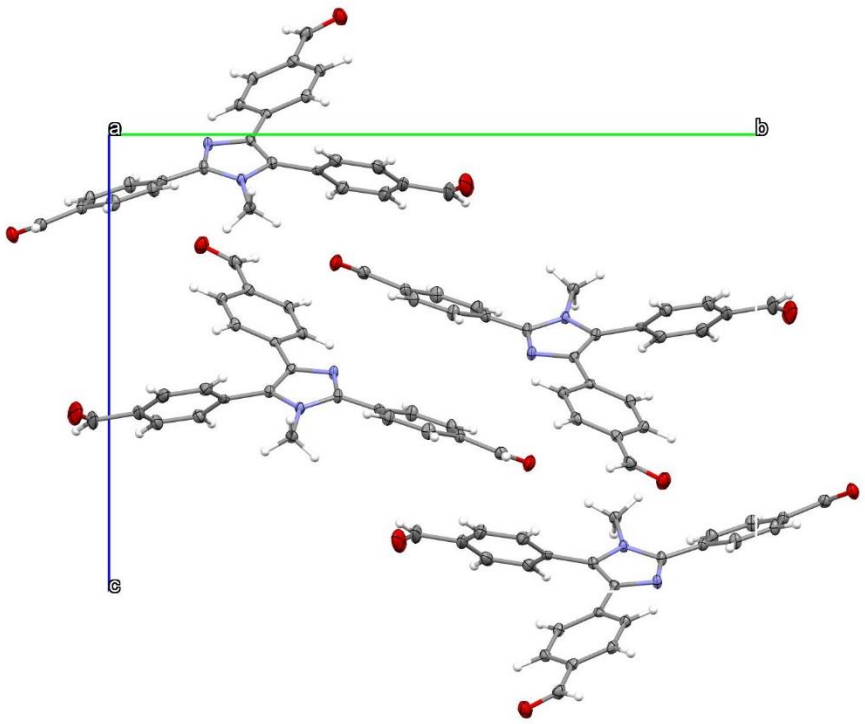

Figure S26. Crystal packing of **1a**, view of unit cell along *a*-axis.

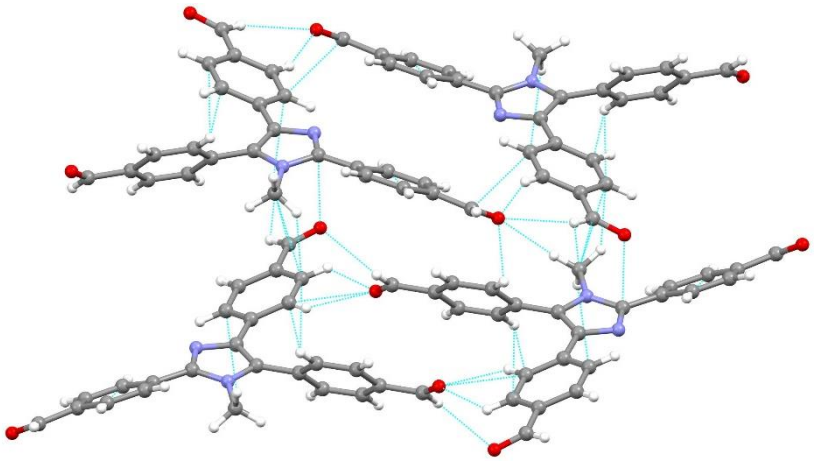

Figure S27. Supramolecular architecture of **1a**, short contacts are presented with light blue lines.

4. Thermal analysis

Thermal properties of imidazoles **1**-**6** were determined by differential scanning calorimetry DSC with a Mettler-Toledo STARe System DSC 2/700 equipped with FRS 6 ceramic sensor and cooling system HUBER TC100-MT RC 23. Thermal behavior of the target compounds was measured in aluminous crucibles sealed with a holed lid under N_2 inert atmosphere (65 ml×min^{-1}). DSC curves were recorded with a scan rate of 5 °C/min within the range of 25–600°C.

Table S2. Thermal characterization of the investigated tripodal imidazoles **1a**–**4a** and **1b**–**6b**.

	Compound	T_m [°C][a]	T_d [°C][b]
Series **a**	**1a**	209	290
	2a	273	> 400
	3a	166	> 400
	4a	199	/
Series **b**	**1b**	/	270
	2b	196	260
	3b	/	330
	4b	/	>220
	5b	/	310
	6b	205	320

[a] T_m = melting point (the point of intersection of a baseline and a tangent of thermal effect = onset).
[b] T_d = temperature of exo(endo)thermic decomposition (a thermal pyrolysis under inert atmosphere).

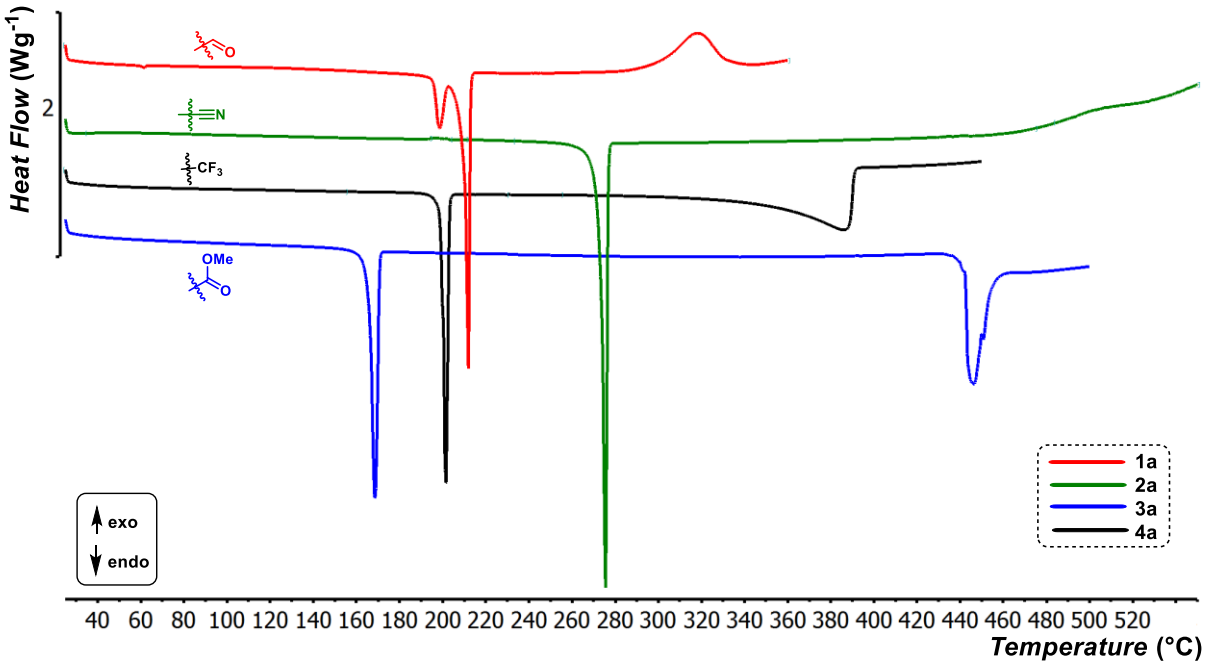

Figure S28. DSC thermograms of tripodal imidazoles in series **a** measured with a scan rate of 5°C/min within the range 25–600 °C.

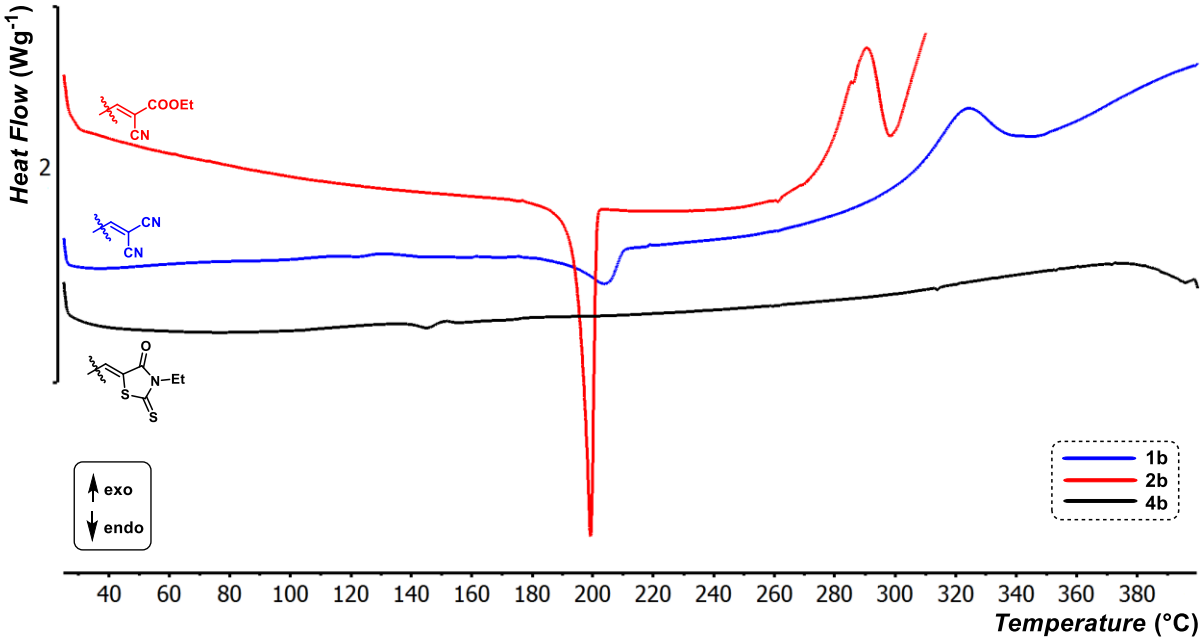

Figure S29. DSC thermograms of tripodal imidazoles in series **b** measured with a scan rate of 5°C/min within the range 25–600 °C.

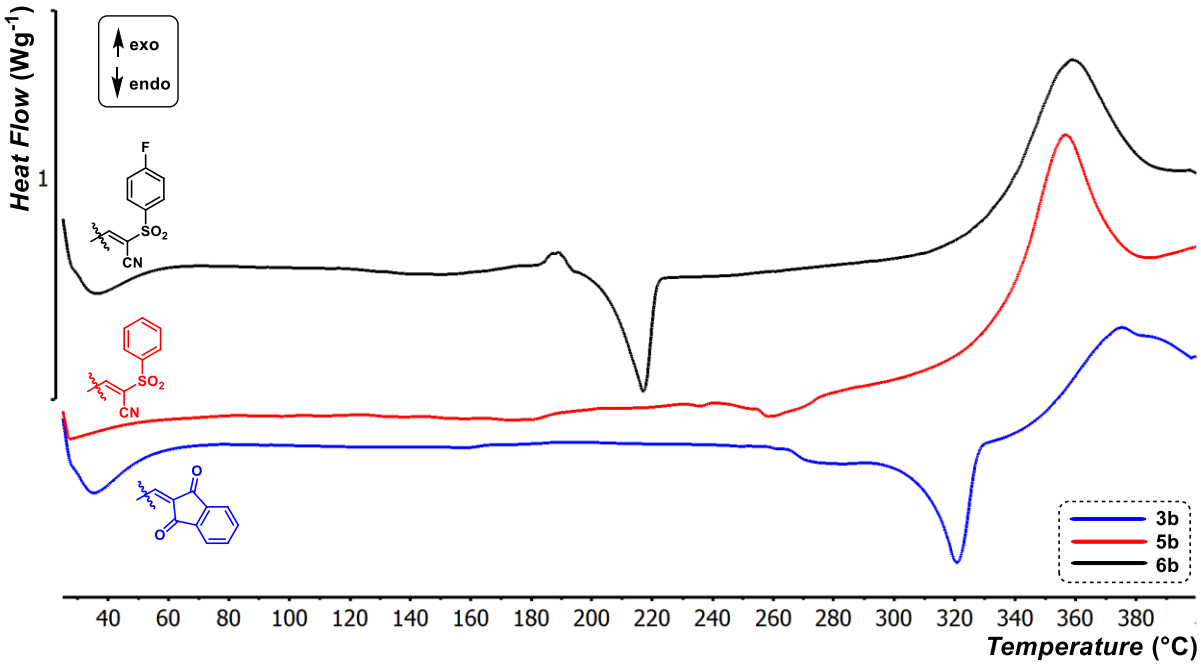

Figure S30. DSC thermograms of tripodal imidazoles in series **b** measured with a scan rate of 5°C/min within the range 25–600 °C.

5. Electrochemistry

The electrochemical behavior of target imidazoles **1**–**6** was investigated in ACN containing 0.1 M Bu_4NPF_6 in a three-electrode cell by cyclic voltammetry (CV). The working electrode was glassy carbon disk (1 mm in diameter). As the reference and auxiliary electrodes were used leakless Ag/AgCl electrode (SSCE) containing filling electrolyte (3.4 M KCl) and titanium rod with a thick coating of platinum, respectively. Voltammetric measurements were performed by using an integrated potentiostat system ER466 (eDAQ Europe) operated with EChem Electrochemistry software. Determined peak potentials of the first oxidation and reduction were assigned from the first cycle at scan rate 100 $mV \cdot s^{-1}$ and were related to the silver/silver chloride electrode (SSCE; +0.205 V vs. SHE). Although the measured solution was bubbled with argon before the voltammetric analysis, the residual peak of oxygen reversible reduction was recorded around –0.7 V vs. SSCE.

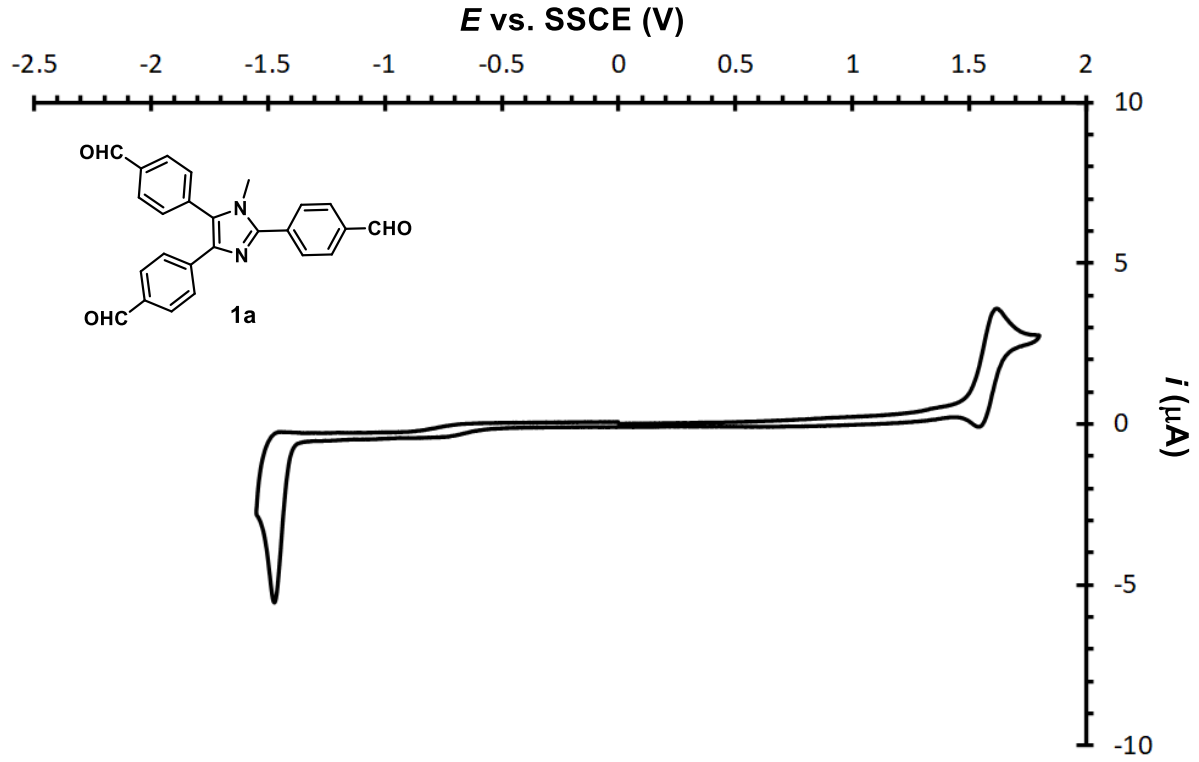

Figure S31. Cyclic voltammogram of chromophore **1a** in ACN containing 0.1 M Bu_4NPF_6 at glassy carbon electrode; v = 100 mVs^{-1}.

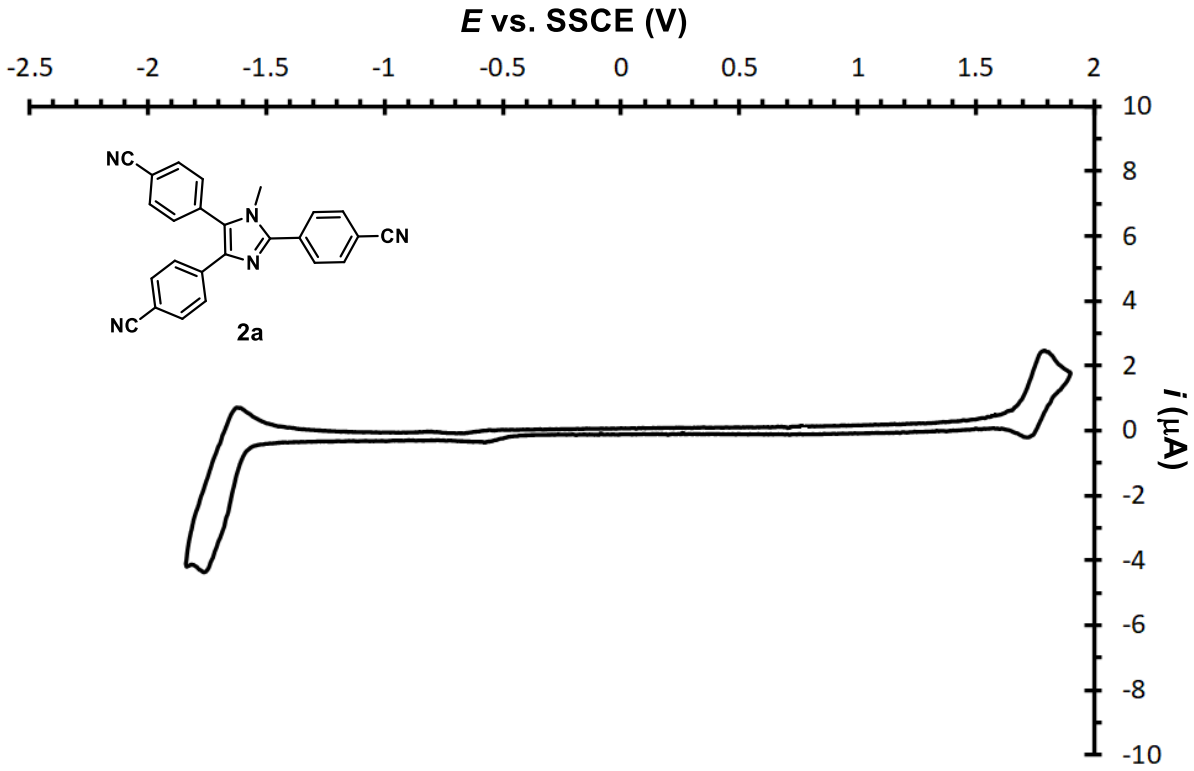

Figure S32. Cyclic voltammogram of chromophore **2a** in ACN containing 0.1 M Bu_4NPF_6 at glassy carbon electrode; v = 100 mVs^{-1}.

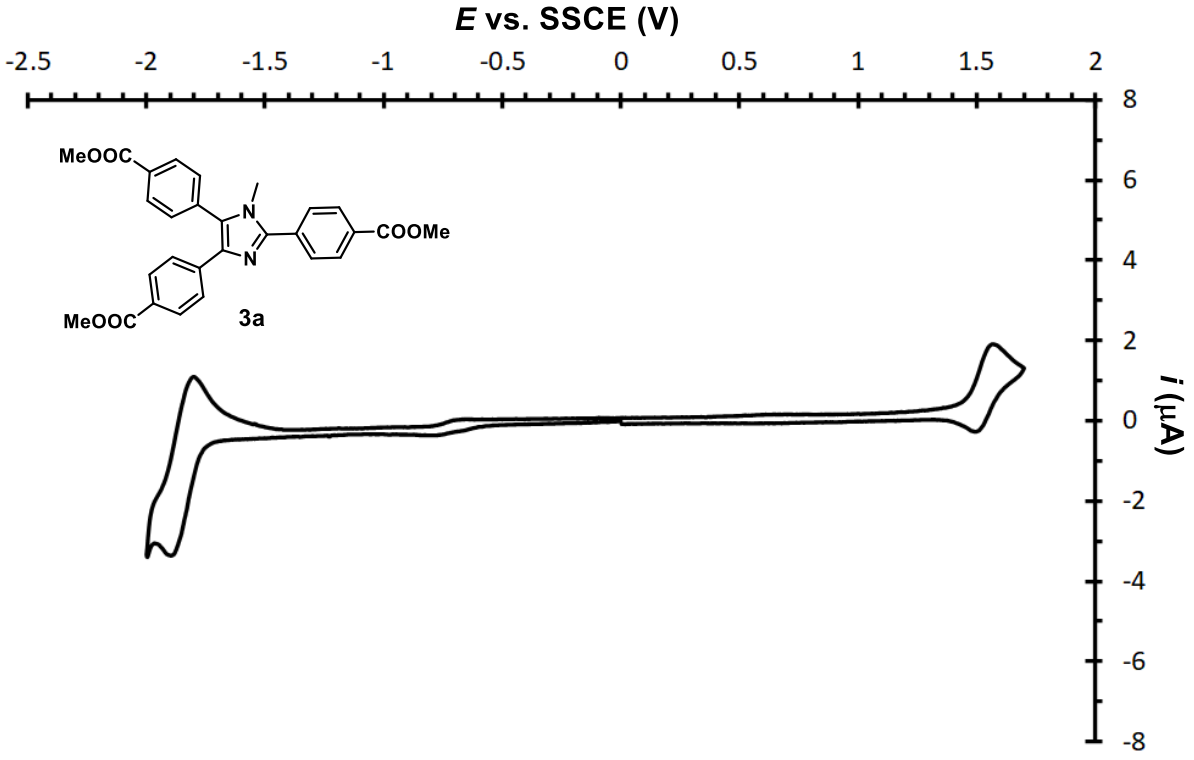

Figure S33. Cyclic voltammogram of chromophore **3a** in ACN containing 0.1 M Bu_4NPF_6 at glassy carbon electrode; v = 100 mVs^{-1}.

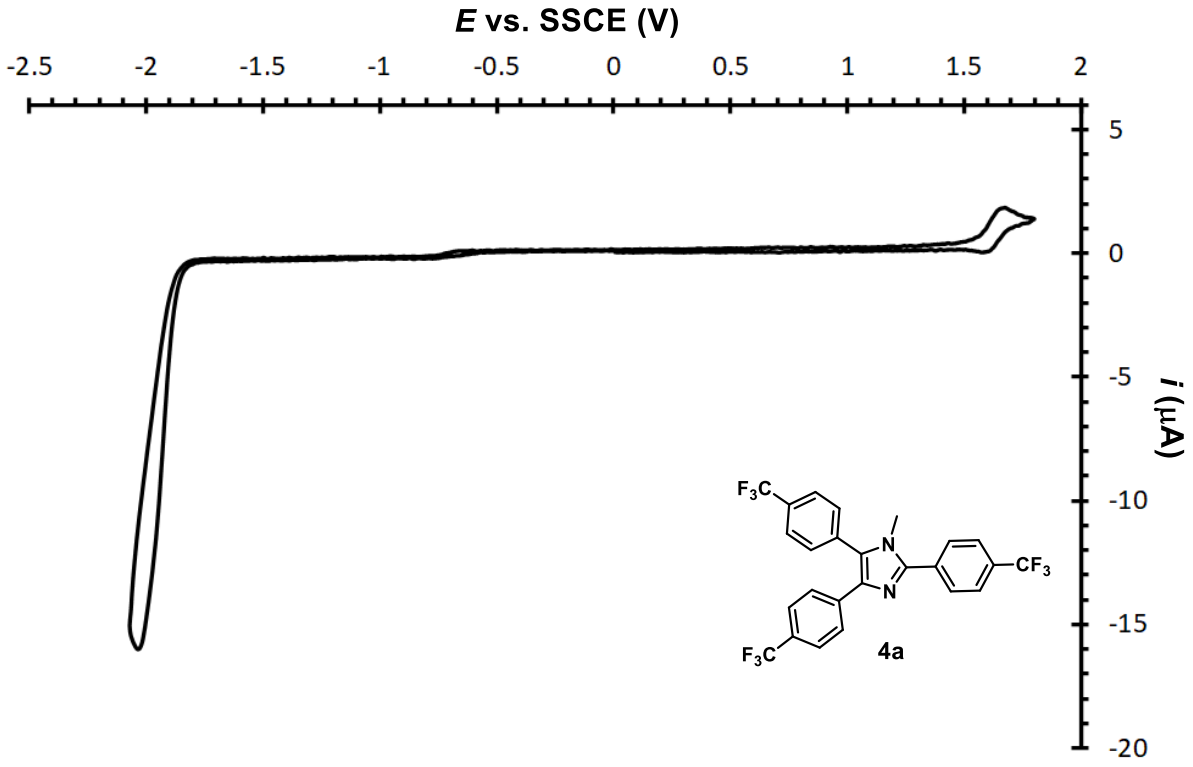

Figure S34. Cyclic voltammogram of chromophore **4a** in ACN containing 0.1 M Bu_4NPF_6 at glassy carbon electrode; v = 100 mVs^{-1}.

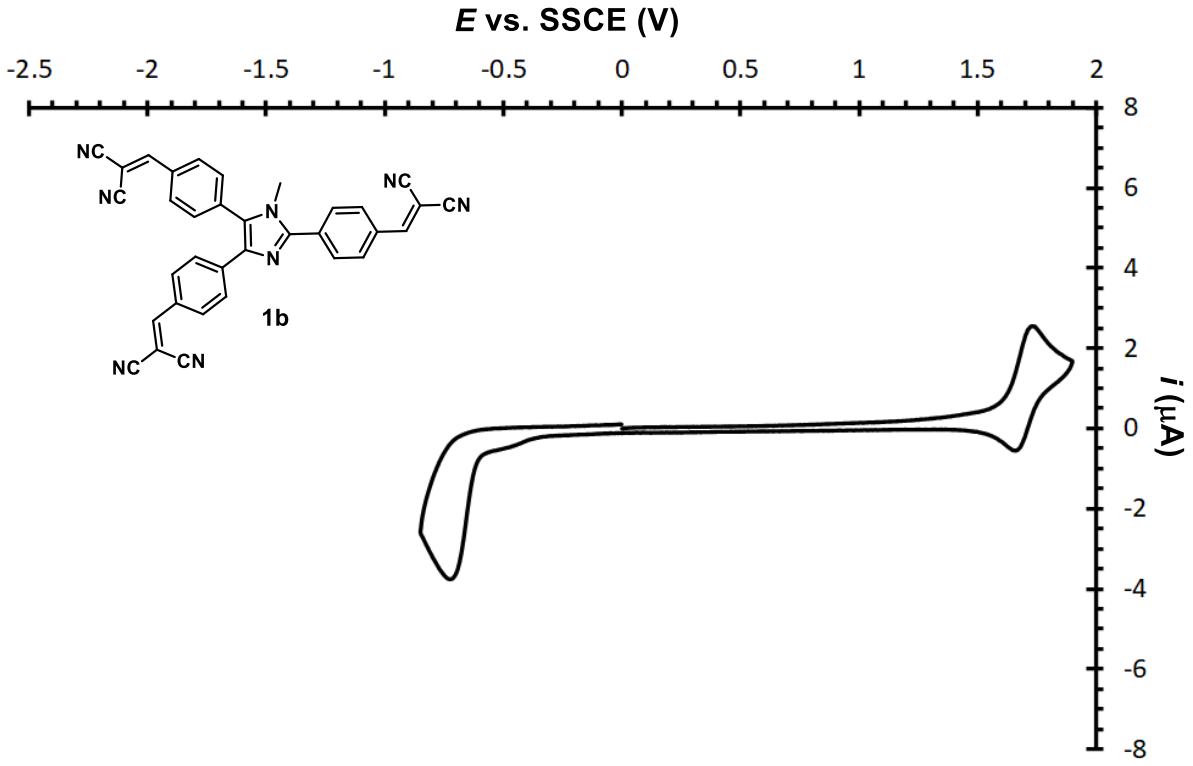

Figure S35. Cyclic voltammogram of chromophore **1b** in ACN containing 0.1 M Bu_4NPF_6 at glassy carbon electrode; v = 100 mVs^{-1}.

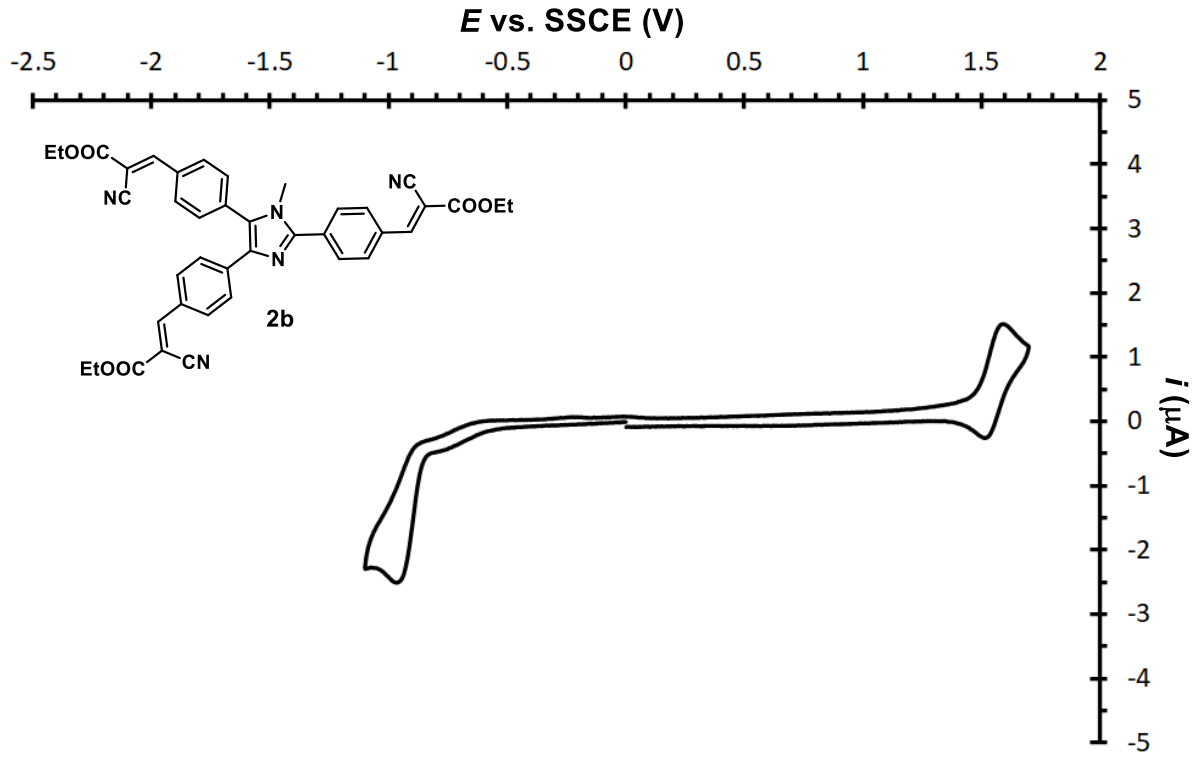

Figure S36. Cyclic voltammogram of chromophore **2b** in ACN containing 0.1 M Bu_4NPF_6 at glassy carbon electrode; v = 100 mVs^{-1}.

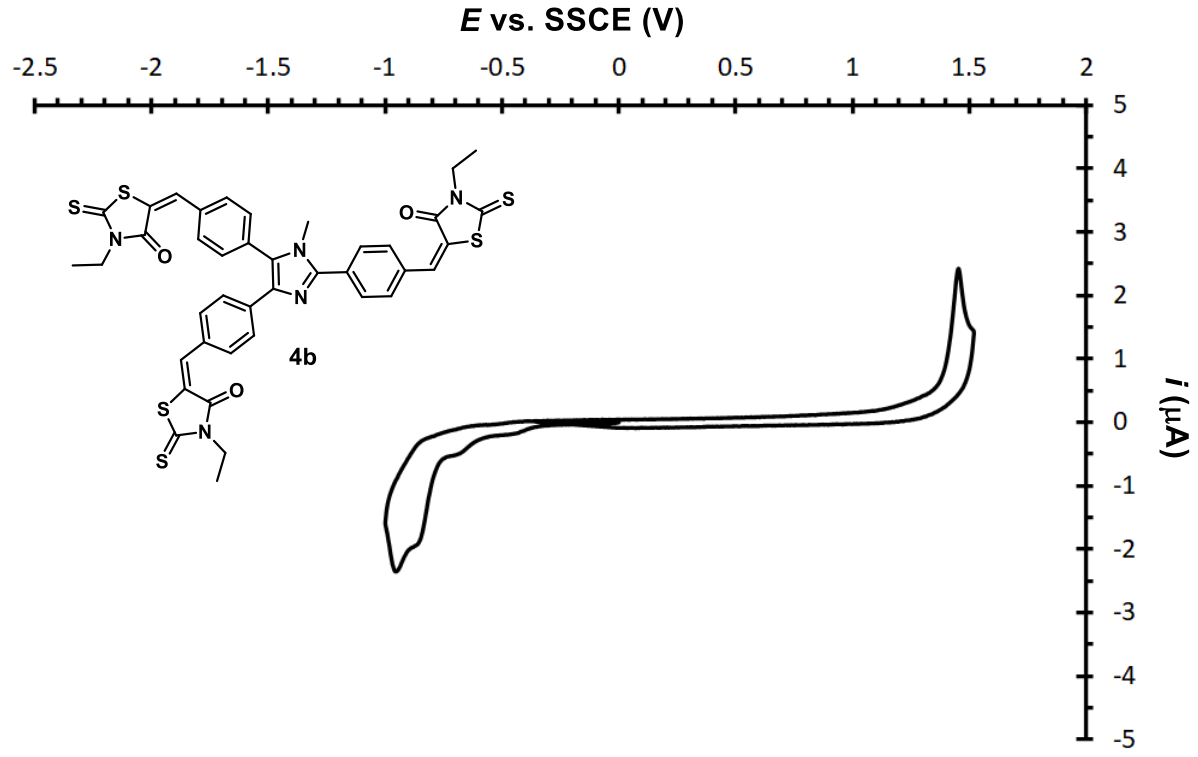

Figure S37. Cyclic voltammogram of chromophore **4b** in ACN containing 0.1 M Bu_4NPF_6 at glassy carbon electrode; v = 100 mVs^{-1}.

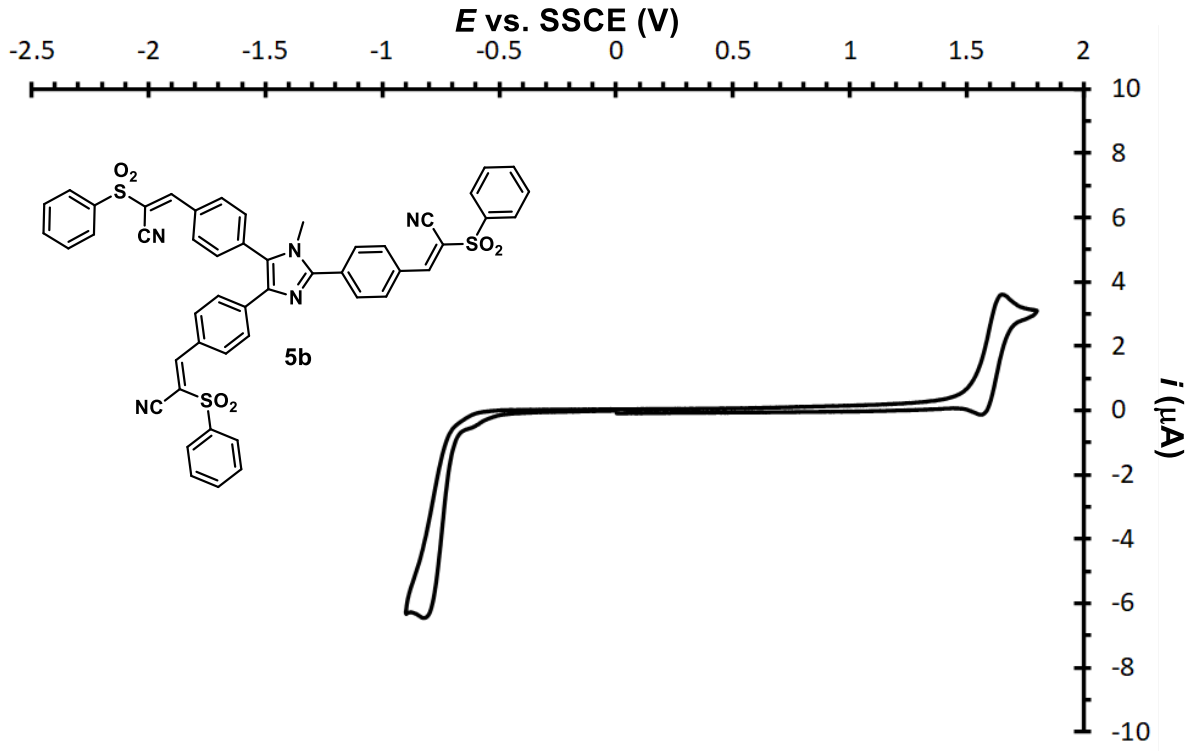

Figure S38. Cyclic voltammogram of chromophore **5b** in ACN containing 0.1 M Bu_4NPF_6 at glassy carbon electrode; v = 100 mVs^{-1}.

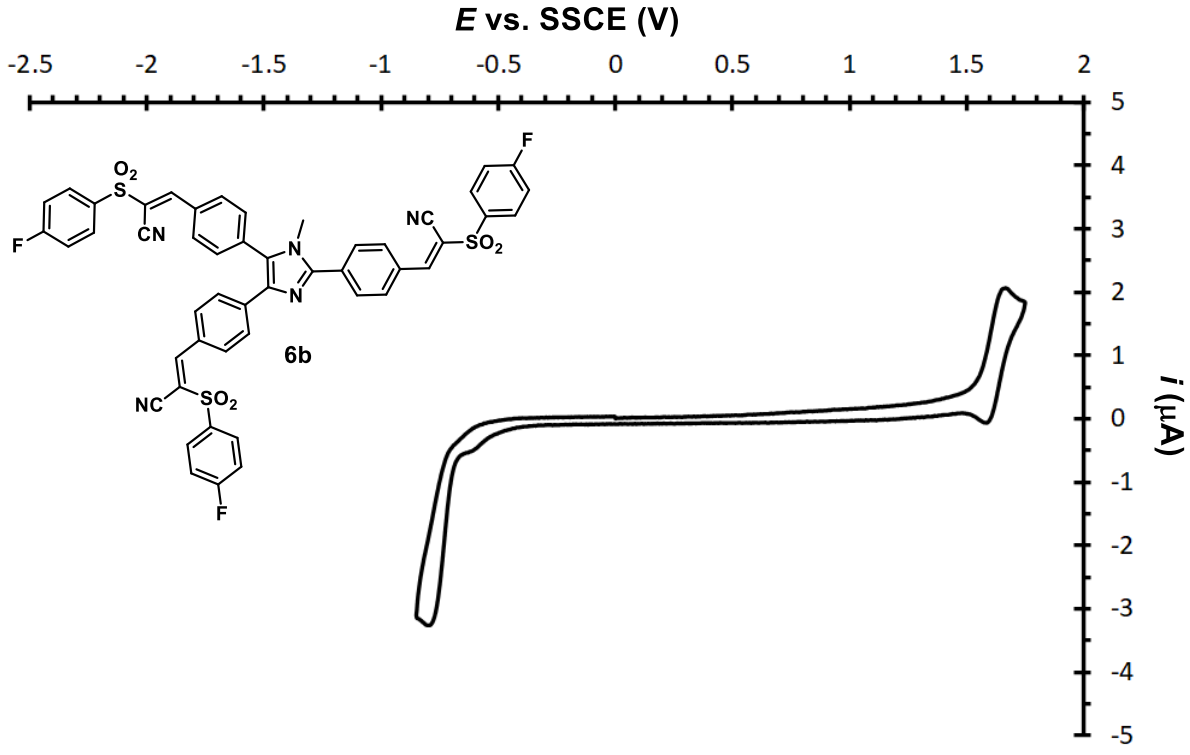

Figure S39. Cyclic voltammogram of chromophore **6b** in ACN containing 0.1 M Bu_4NPF_6 at glassy carbon electrode; v = 100 mVs^{-1}.

6. Linear optical properties

Absorption and photoluminescence spectra were measured on a Duetta™ HORIBA spectrophotometer at room temperature. To record their emission spectra, imidazoles **1a**–**4a** and **1b**–**6b** were excited at their longest-wavelength absorption maxima λ_{max}^{A}. Fluorescence quantum yields (±10%) of **1a**–**4a** and **1b**–**6b** were determined relative to that of anthracene (Φ_f = 0.36 in cyclohexane) and perylene (Φ_f = 0.94 in cyclohexane) used as internal standard, respectively.[8]

Table S3. Optical properties of imidazole-centred chromophores **1**–**6** in toluene.

Comp	λ_{max}^{A} [nm/eV]	ε [$M^{-1}cm^{-1}$]	λ_{max}^{E} [nm/eV]	Φ [%]	*Stokes shift* [cm^{-1}/eV]
1a	345/3.59	30 500	439/2.82	10	6210/0.77
2a	325/3.82	28 800	417/2.97	42	6790/0.85
3a	329/3.77	36 500	422/2.94	42	6700/0.83
4a	304/4.08	23 500	390/3.18	37	7250/0.90
1b	410/3.02	45 400	517/2.40	60	5050/0.62
2b	401/3.09	52 200	511/2.43	61	5370/0.66
4b	429/2.89	78 600	531/2.34	<1	4480/0.55
5b	405/3.06	42 800	518/2.39	59	5390/0.67
6b	407/3.05	49 600	518/2.39	55	5270/0.66

Table S4. Optical properties of imidazole-centred chromophores **1**–**6** in $CHCl_3$.

Comp	λ_{max}^{A} [nm/eV]	ε [$M^{-1}cm^{-1}$]	λ_{max}^{E} [nm/eV]	Φ [%]	*Stokes shift* [cm^{-1}/eV]
1a	342/3.63	39 400	459/2.70	38	7450/0.93
2a	321/3.86	31 800	417/2.97	45	7170/0.89
3a	324/3.83	37 800	427/2.90	42	7440/0.93
4a	299/4.15	22 950	389/3.19	42	7740/0.96
1b	410/3.02	43 700	540/2.29	47	5870/0.73
2b	396/3.13	47 100	538/2.30	45	6670/0.83
3b	447/2.77	64 100	603/2.06	8	5790/0.71
4b	425/2.92	77 200	573/2.16	4	6080/0.76
5b	401/3.09	51 300	545/2.28	56	6590/0.81
6b	402/3.08	49 300	545/2.28	53	6530/0.80

[8] A. M. Brouwer, *Pure Appl. Chem.*, 2011, **83**, 2213.

Table S5. Optical properties of imidazole-centred chromophores **1**–**6** in ACN.

Comp	λ_{max}^{A} [nm/eV]	ε [$M^{-1}cm^{-1}$]	λ_{max}^{E} [nm/eV]	Φ [%]	*Stokes shift* [cm^{-1}/eV]
1a	342/3.63	32 800	487/2.55	43	8700/1.08
2a	322/3.85	35 000	426/2.91	35	7580/0.94
3a	323/3.84	40 500	437/2.84	42	8080/1.00
4a	301/4.12	24 300	395/3.14	40	7910/0.98
1b	405/3.06	35 600	617/2.01	3	8480/1.05
2b	392/3.16	42 900	603/2.06	3	8930/1.10
4b	419/2.96	70 600	647/1.92	2	8410/1.04
5b	401/3.09	54 600	625/1.98	2	8938/1.11
6b	402/3.08	43 300	622/1.99	1	8798/1.09

Table S6. Fitting parameters of the nanosecond fluorescence dynamics of **1b**–**6b** in toluene. The dynamics were detected at the peaks of the fluorescence spectra.

Comp	A_1	τ_1 [ns]	A_2	τ_2 [ns]	A_3	τ_3 [ns]	$\langle\tau\rangle$ [ns]	χ^2
1b	-	-	0.61	0.73	0.39	2.56	1.44	1.03
2b	-	-	0.25	0.58	0.75	2.28	1.85	1.02
4b	1.00	0.17	-	-	-	-	0.17	0.89
5b	-	-	0.56	1.21	0.44	2.83	1.92	1.06
6b	-	-	0.31	1.02	0.69	2.64	2.14	1.00

Table S7. Fitting parameters of the nanosecond fluorescence dynamics of **1b**–**6b** in $CHCl_3$. The dynamics were detected at the peaks of the fluorescence spectra.

Comp	A_1	τ_1 [ns]	A_2	τ_2 [ns]	A_3	τ_3 [ns]	$\langle\tau\rangle$ [ns]	χ^2
1b	0.34	0.12	0.57	0.65	0.09	3.00	0.67	0.99
2b	0.17	0.12	0.93	1.67	0.63	2.83	1.99	0.98
3b	0.58	0.44	0.81	1.53	-	-	0.60	0.84
4b	0.43	0.17	0.57	0.89	-	-	0.58	0.76
5b	0.26	0.33	0.65	1.43	0.09	4.08	1.36	0.99
6b	0.14	0.38	0.50	1.52	0.36	3.67	2.15	0.99

Table S8. Fitting parameters of the nanosecond fluorescence dynamics of **1b**–**6b** in THF. The dynamics were detected at the peaks of the fluorescence spectra.

Comp	A_1	τ_1 [ns]	A_2	τ_2 [ns]	A_3	τ_3 [ns]	$\langle\tau\rangle$ [ns]	χ^2
1b	0.17	0.64	0.68	1.97	0.15	4.06	2.04	1.01
2b	-	-	0.21	0.92	0.79	3.37	2.85	1.00
3b	-	-	0.28	0.93	0.72	1.53	1.36	1.07
4b	0.36	0.23	0.50	1.82	0.14	2.44	1.34	1.02
5b	-	-	0.49	1.79	0.51	3.69	2.76	1.06
6b	-	-	0.23	1.57	0.77	3.74	3.23	1.00

Table S9. Fitting parameters of the nanosecond fluorescence dynamics of **1b**–**6b** in ACN. The dynamics were detected at the peaks of the fluorescence spectra.

Comp	A_1	τ_1 [ns]	A_2	τ_2 [ns]	A_3	τ_3 [ns]	$\langle\tau\rangle$ [ns]	χ^2
1b	-	-	0.17	0.70	0.83	1.39	1.27	0.95
2b	-	-	0.31	0.68	0.69	1.23	1.05	0.96
3b	0.76	0.25	0.24	0.54	-	-	0.32	0.94
4b	0.28	0.29	0.72	1.03	-	-	0.82	0.88
5b	-	-	0.71	0.94	0.29	1.82	1.20	1.01
6b	-	-	0.75	0.63	0.25	1.28	0.79	0.94

Table S10. Fitting parameters of the nanosecond fluorescence dynamics of **2b, 5b** and **6b** in THF at various emission wavelengths.

Comp	λ (nm)	A_1	τ_1 [ns]	A_2	τ_2 [ns]	<τ> [ns]	χ^2
2b/THF	**500**	0.24	0.96	0.76	3.38	2.79	0.96
	520	0.22	0.96	0.78	3.38	2.84	0.97
	560	0.21	0.96	0.79	3.38	2.87	0.97
	590	0.21	0.96	0.79	3.38	2.87	0.98
	630	0.21	0.96	0.79	3.38	2.88	1.00
	660	0.20	0.96	0.80	3.38	2.88	1.05

Comp	λ (nm)	A_1	τ_1 [ns]	A_2	τ_2 [ns]	<τ> [ns]	χ^2
5b/THF	**500**	0.29	1.53	0.71	3.90	3.22	1.02
	520	0.24	1.53	0.76	3.90	3.33	1.02
	540	0.21	1.53	0.79	3.90	3.41	1.05
	573	0.18	1.53	0.82	3.90	3.47	0.95
	590	0.17	1.53	0.83	3.90	3.49	0.99
	630	0.15	1.53	0.85	3.90	3.54	0.99
	660	0.14	1.53	0.86	3.90	3.57	0.99

Comp	λ (nm)	A_1	τ_1 [ns]	A_2	τ_2 [ns]	<τ> [ns]	χ^2
6b/THF	**500**	0.17	1.21	0.83	3.85	3.39	1.02
	520	0.14	1.21	0.86	3.85	3.46	1.03
	540	0.13	1.21	0.87	3.85	3.49	0.98
	580	0.12	1.21	0.88	3.85	3.52	0.98
	590	0.11	1.21	0.89	3.85	3.55	1.00
	630	0.10	1.21	0.90	3.85	3.59	0.97
	660	0.09	1.21	0.91	3.85	3.61	1.00

Table S11. Calculated values of the difference of the permanent dipole moments between the ground and excited states for **1b**-**6b** in THF by using the $\delta_{2PA}(0-0)$ values.

Comp	$\Delta\mu_{2PA}$ (D)
1b	12.8
2b	16.0
3b	13.5
4b	15.9
5b	15.4
6b	17.4

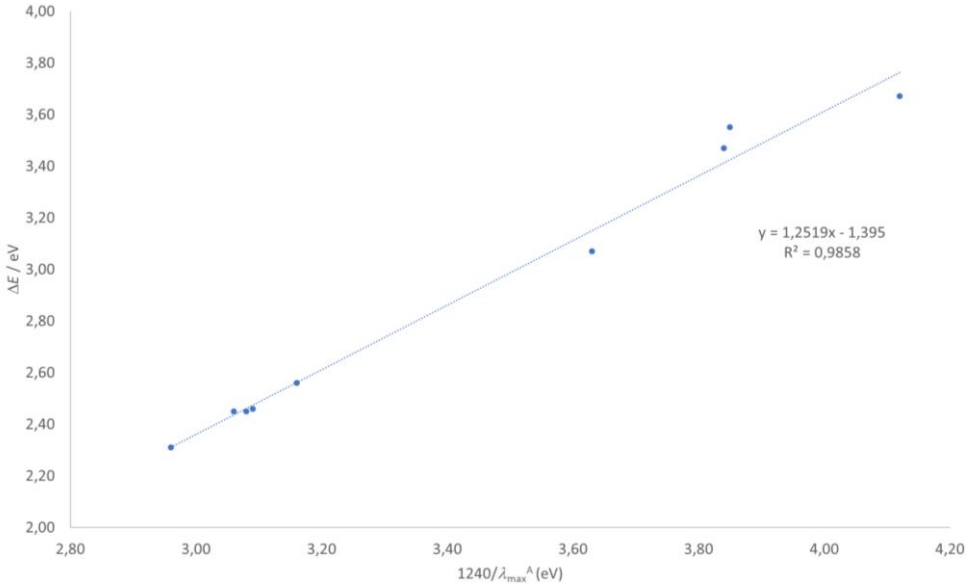

Figure S40. Correlation of the experimental optical (1240/λ_{max}^{A}) and electrochemical (ΔE) gaps.

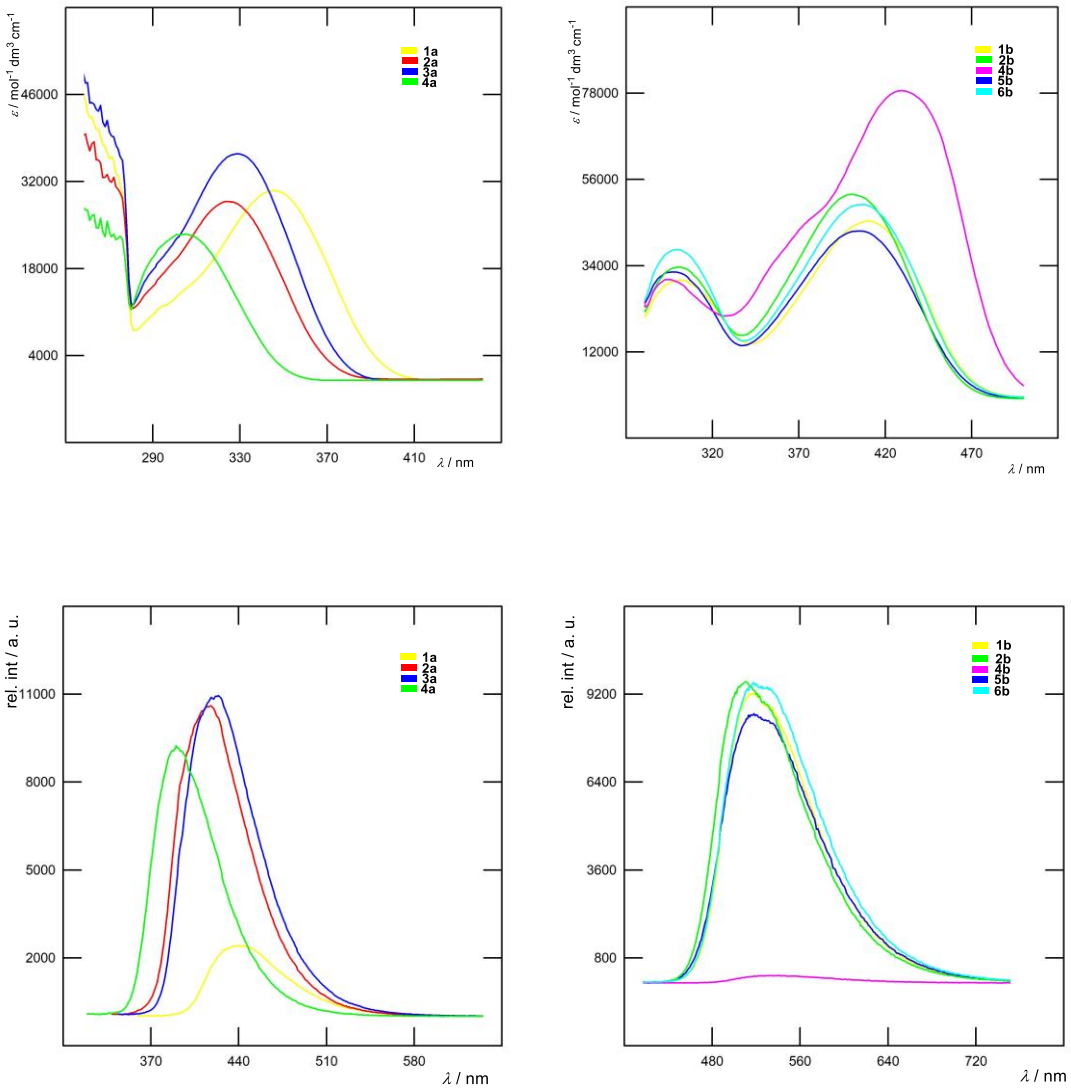

Figure S41. UV-Vis absorption (up) and fluorescence (down) spectra of **1**–**6** in toluene (c = 1×10^{-5} M).

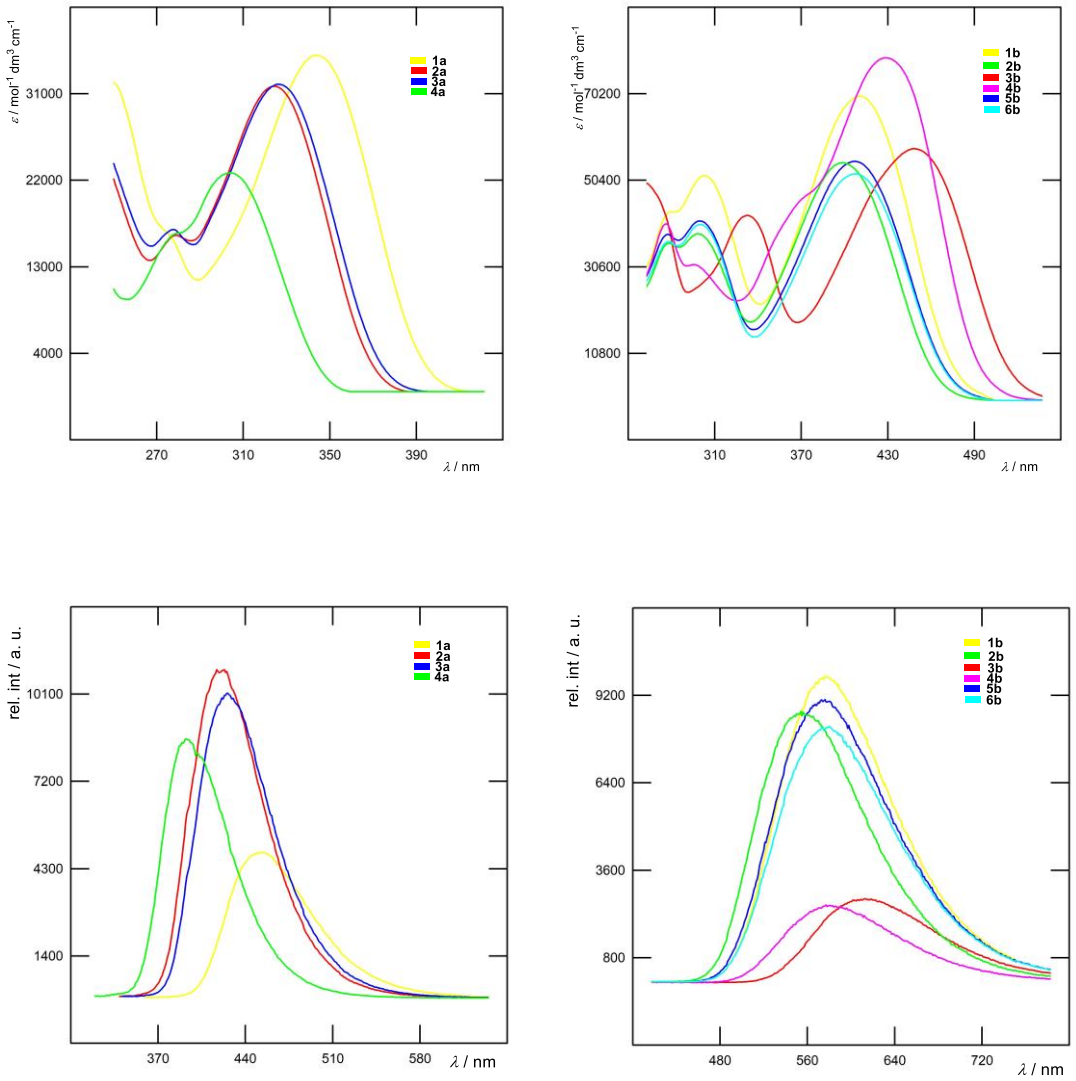

Figure S42. UV-Vis absorption (up) and fluorescence (down) spectra of **1**–**6** in THF (c = 1×10^{-5} M).

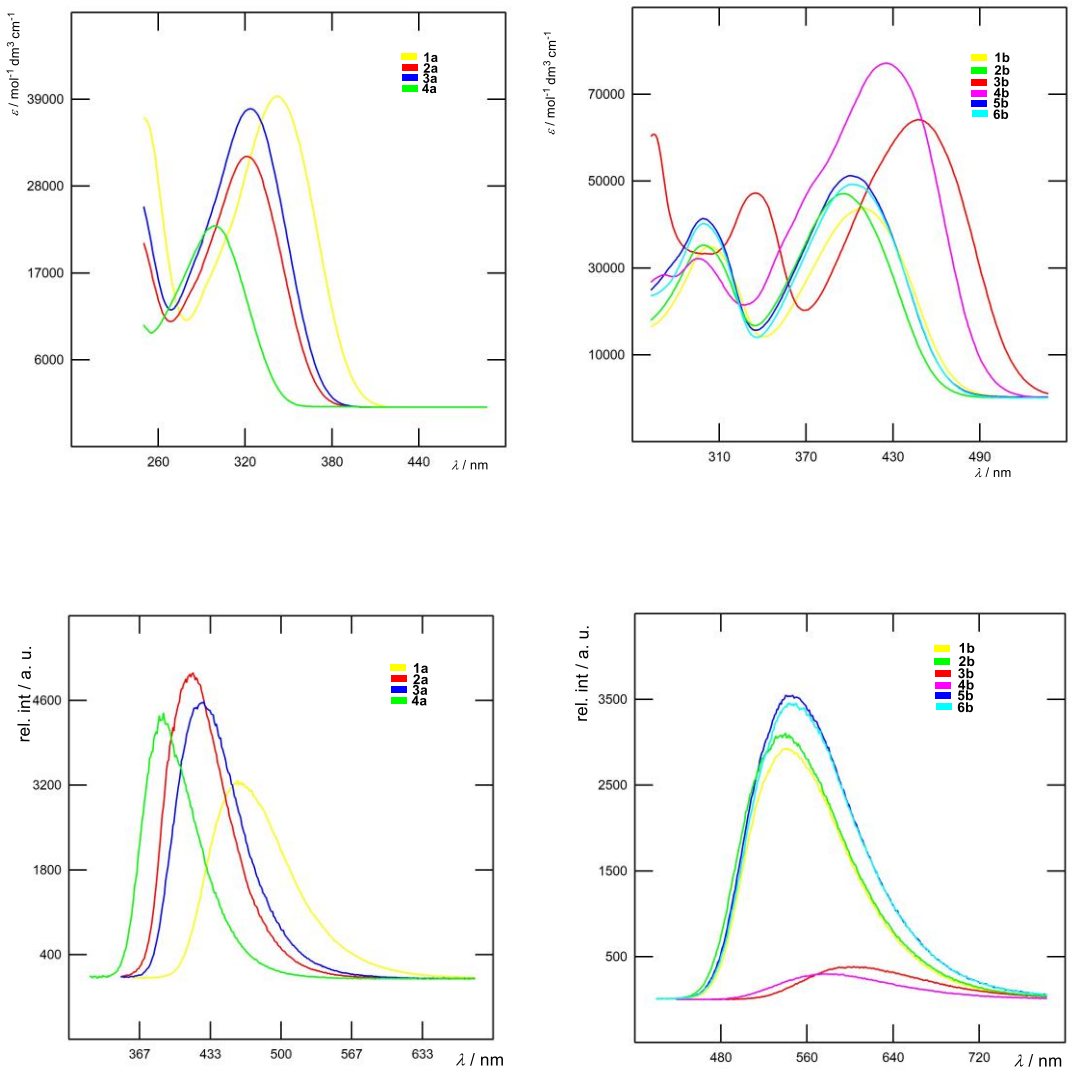

Figure S43. UV-Vis absorption (up) and fluorescence (down) spectra of **1**–**6** in $CHCl_3$ (c = 1×10^{-5} M).

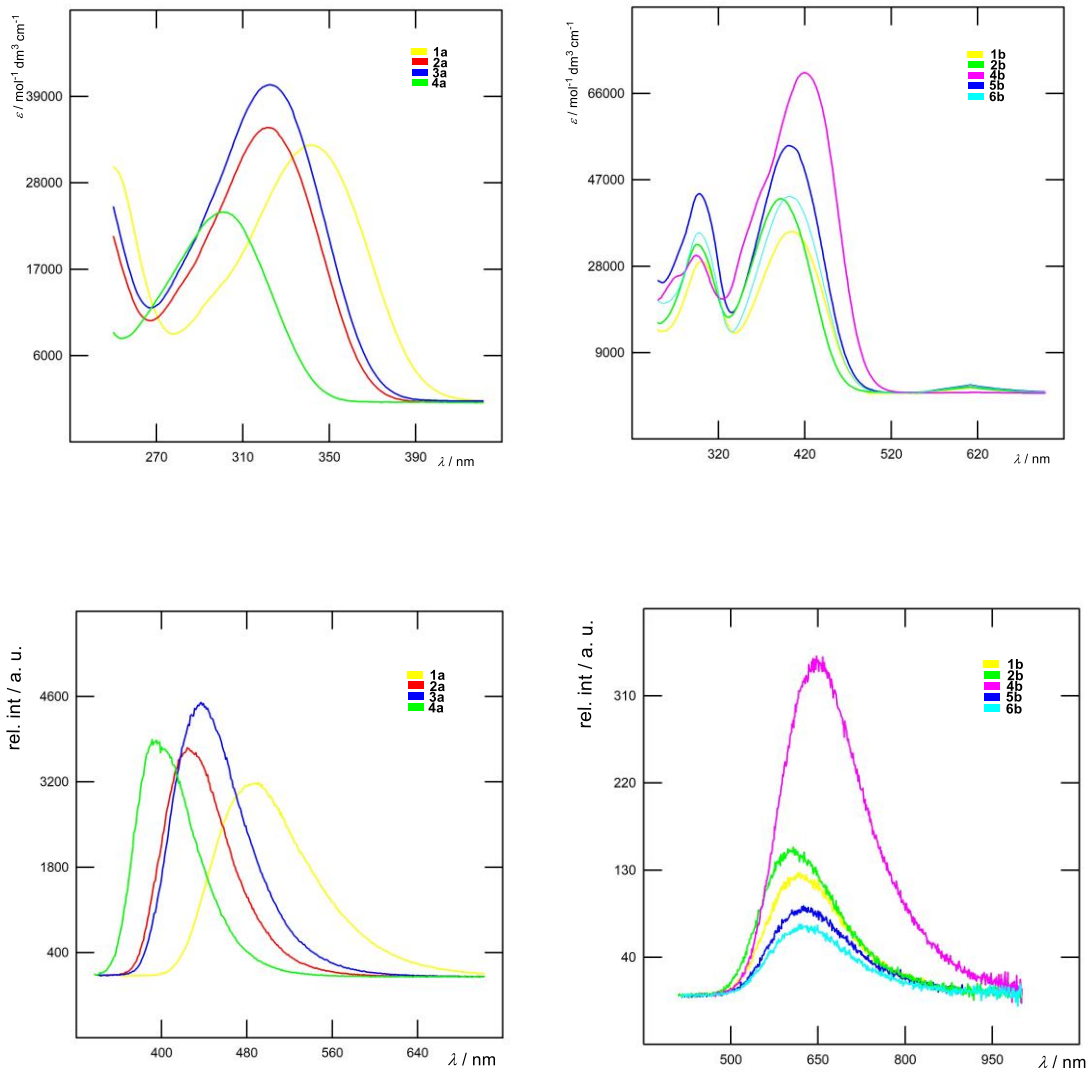

Figure S44. UV-Vis absorption (up) and fluorescence (down) spectra of **1**–**6** in ACN (c = 1×10^{-5} M).

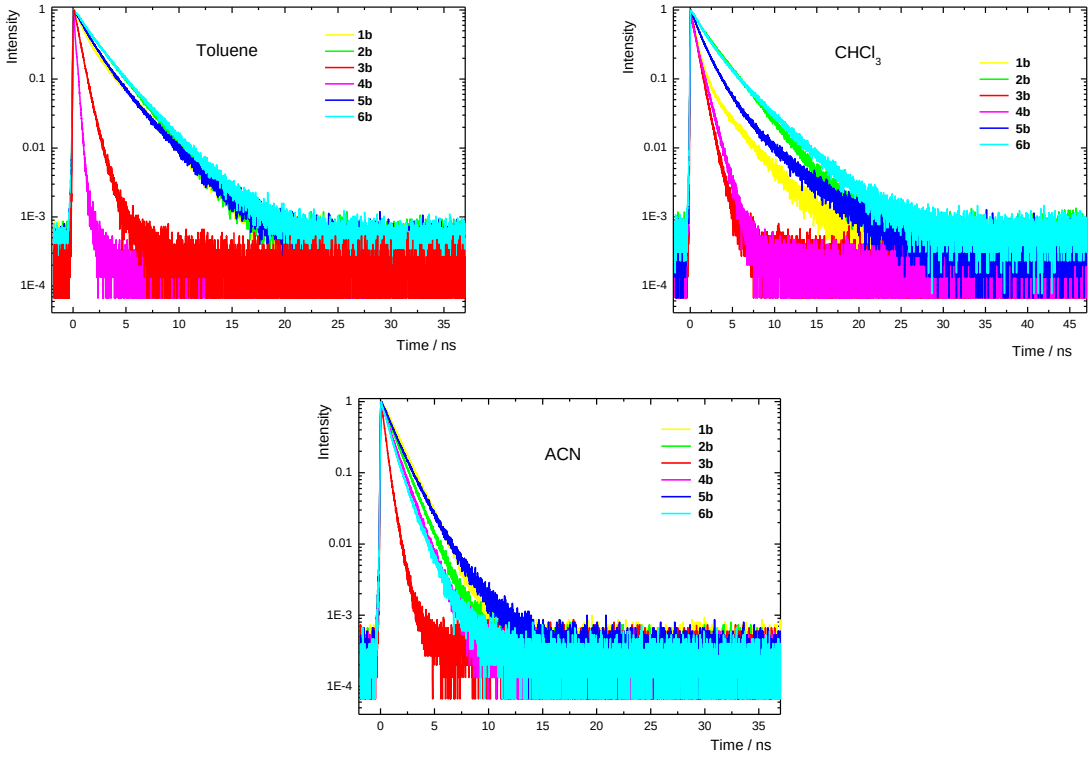

Figure S45. Fluorescence dynamics in the nanosecond timescale of imidazole chromophores measured in toluene, $CHCl_3$ and ACN. The dynamics were detected at the peaks of the fluorescence spectra.

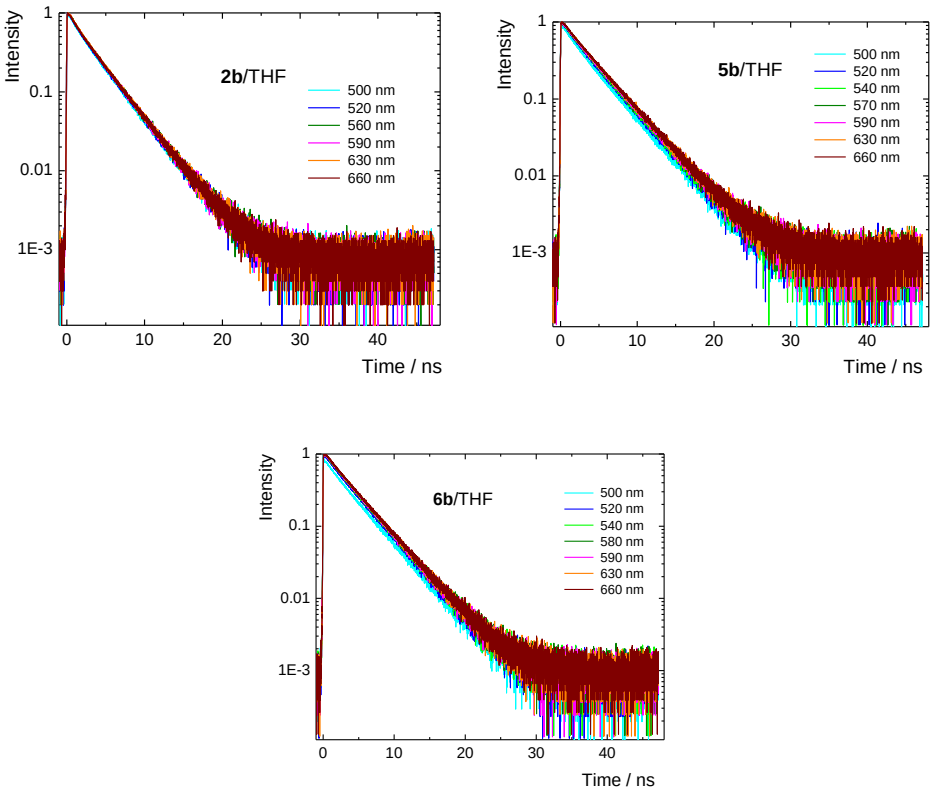

Figure S46. Fluorescence dynamics in the nanosecond timescale of imidazole chromophores **2b**, **5b** and **6b** measured in THF at various emission wavelengths.

7. DFT calculations

The optimized structures of **1**–**6** were obtained via DFTB3LYP/6-311+G(2d,f,p) and DFT B3LYP/6-311+G(2d,p) methods for **5b**/**6b** and other molecules in ACN.

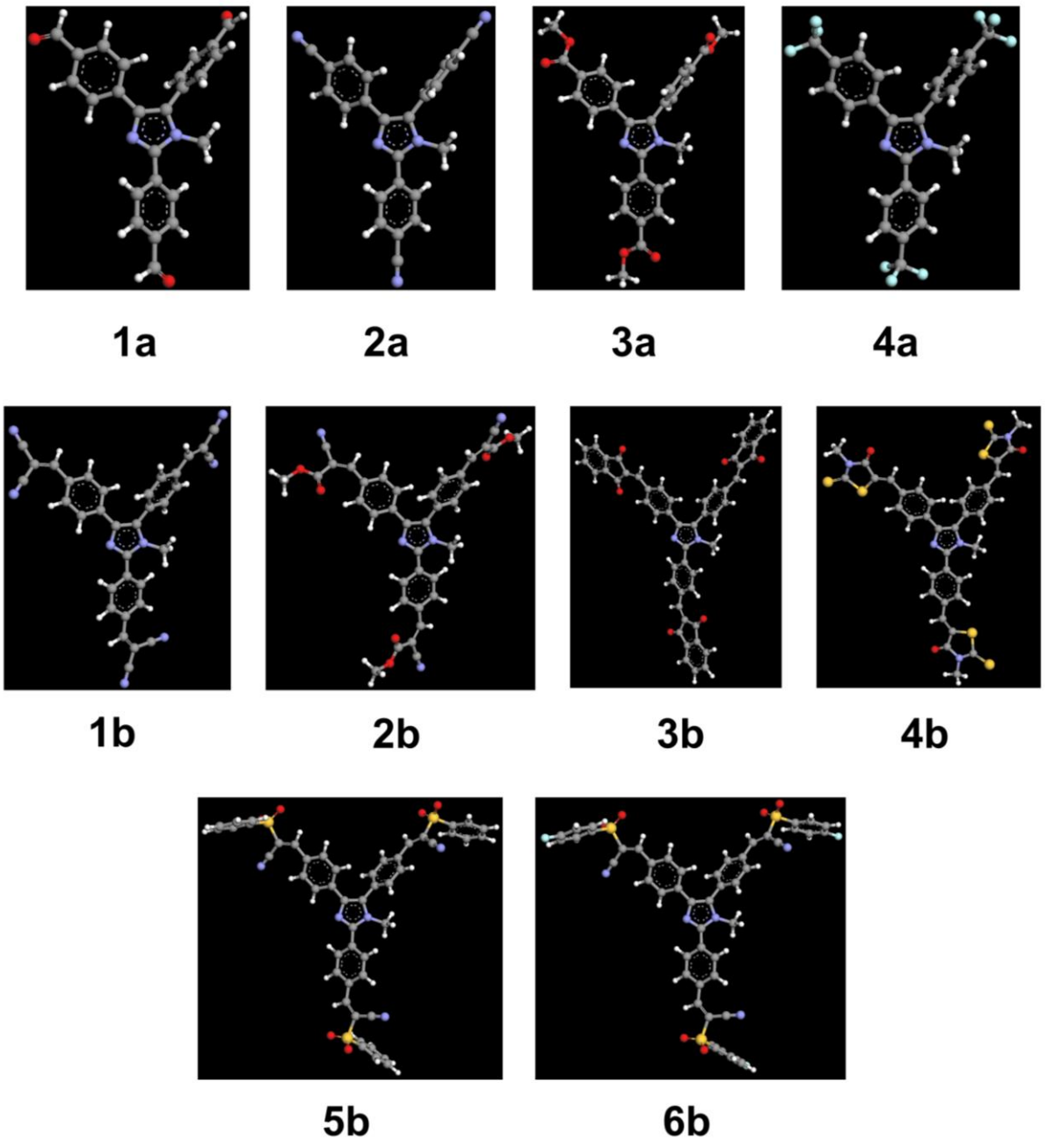

Figure S47. DFT-optimized geometries of target imidazole derivatives **1**–**6**.

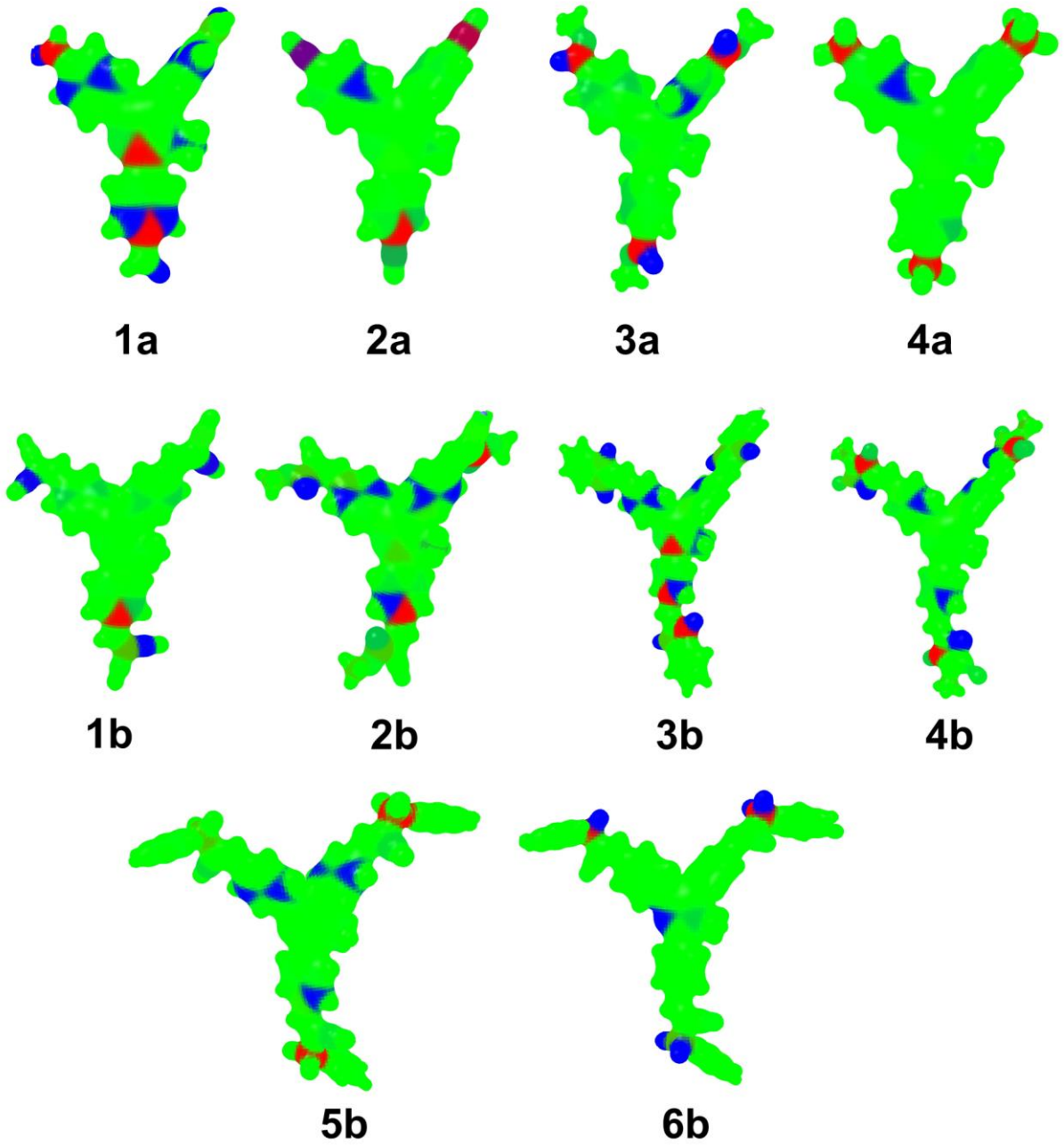

Figure S48. DFT-calculated ESP charges in target imidazole derivatives **1**–**6** (green – neutral, blue – positive, red – negative).

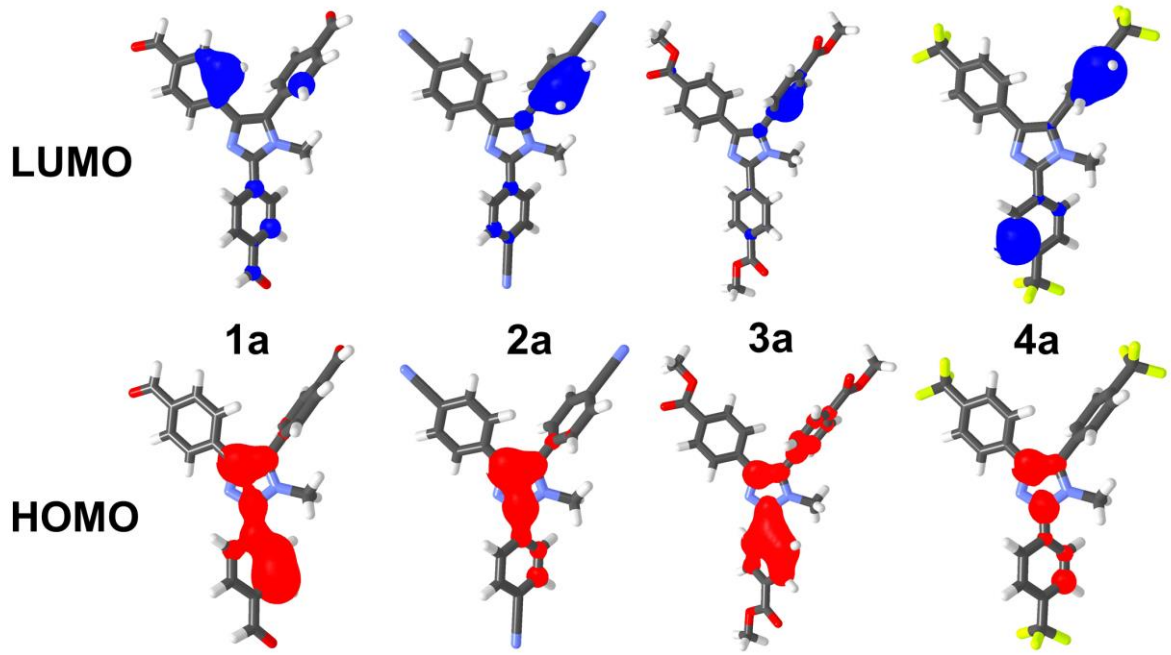

Figure S49. DFT-calculated HOMO (red) and LUMO (blue) localization in imidazole derivatives **1a**–**4a**.

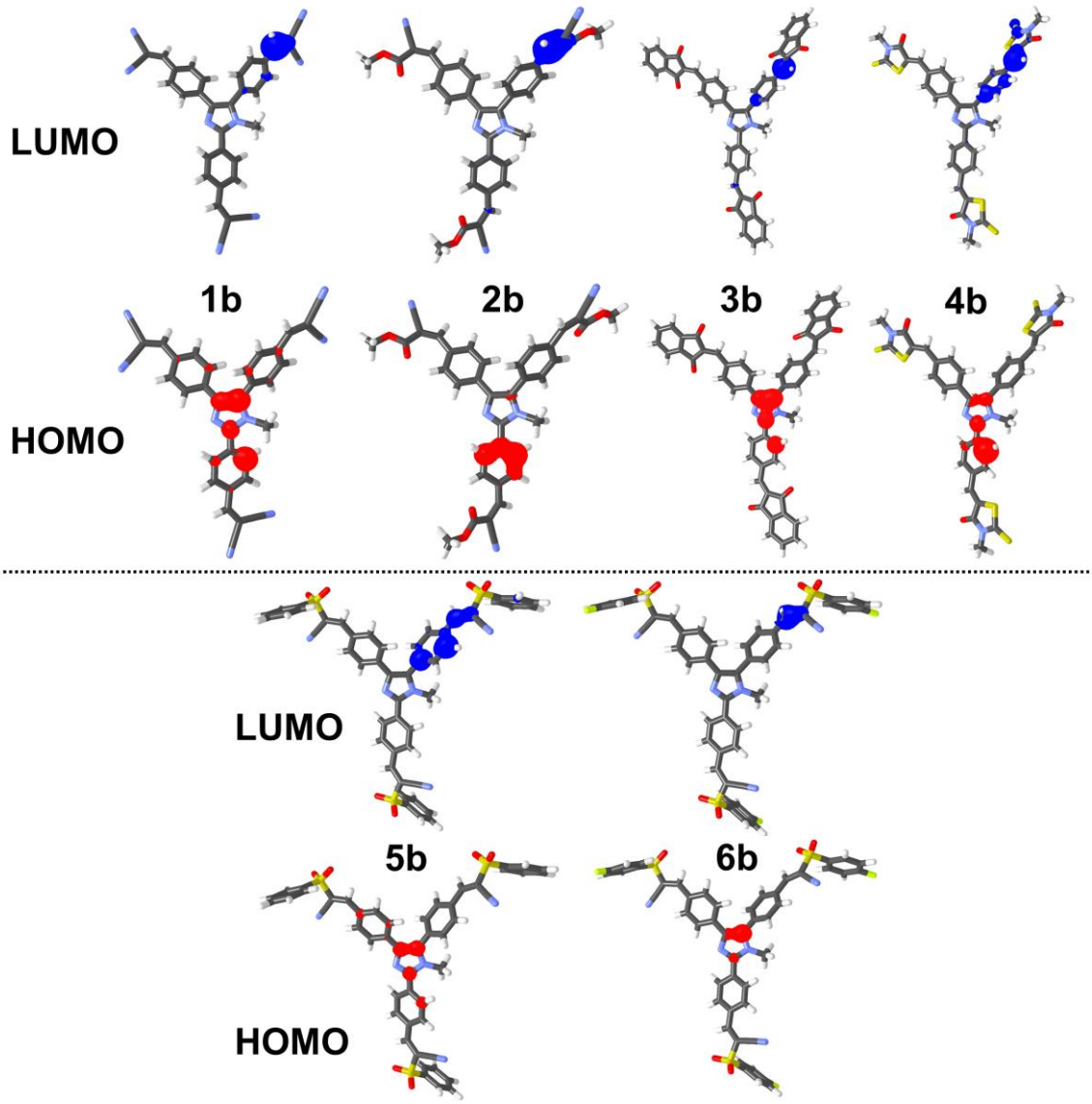

Figure S50. DFT-calculated HOMO (red) and LUMO (blue) localization in imidazole derivatives **1b**–**6b**.

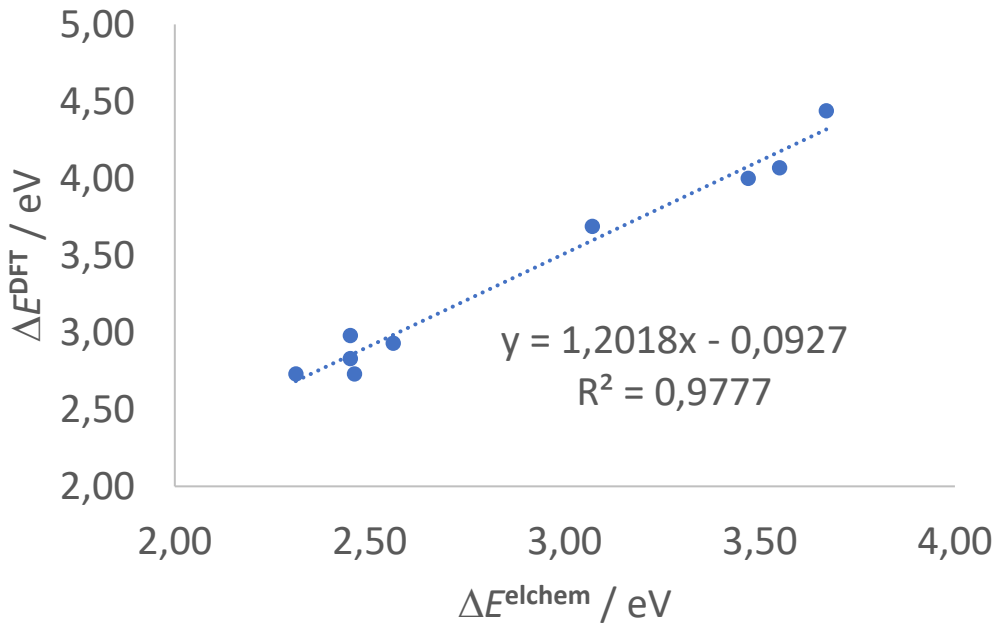

Figure S51. Correlation of the electrochemical (ΔE^{elchem}) and DFT-calculated (ΔE^{DFT}) gaps.

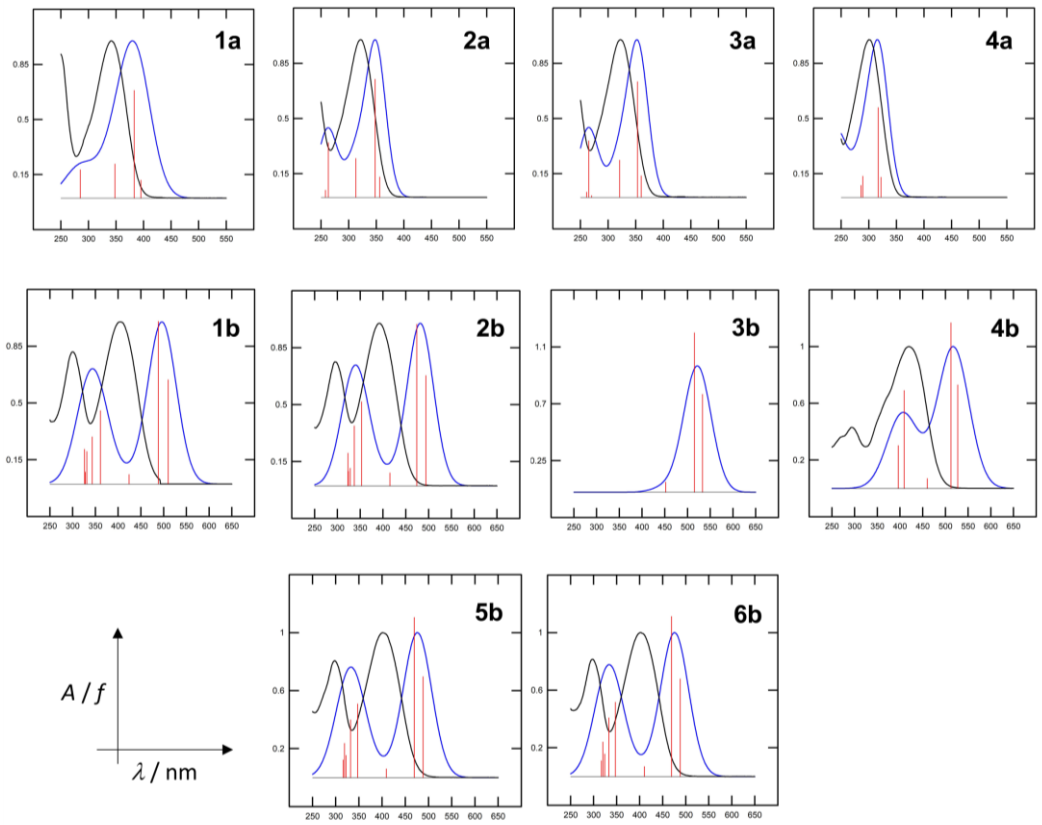

Figure S52. TD-DFT calculated (B3LYP/6-311+g(2df,p), blue) along with experimental (black) UV-Vis absorption spectra in ACN. The red vertical lines represent oscillator strengths (*f*).

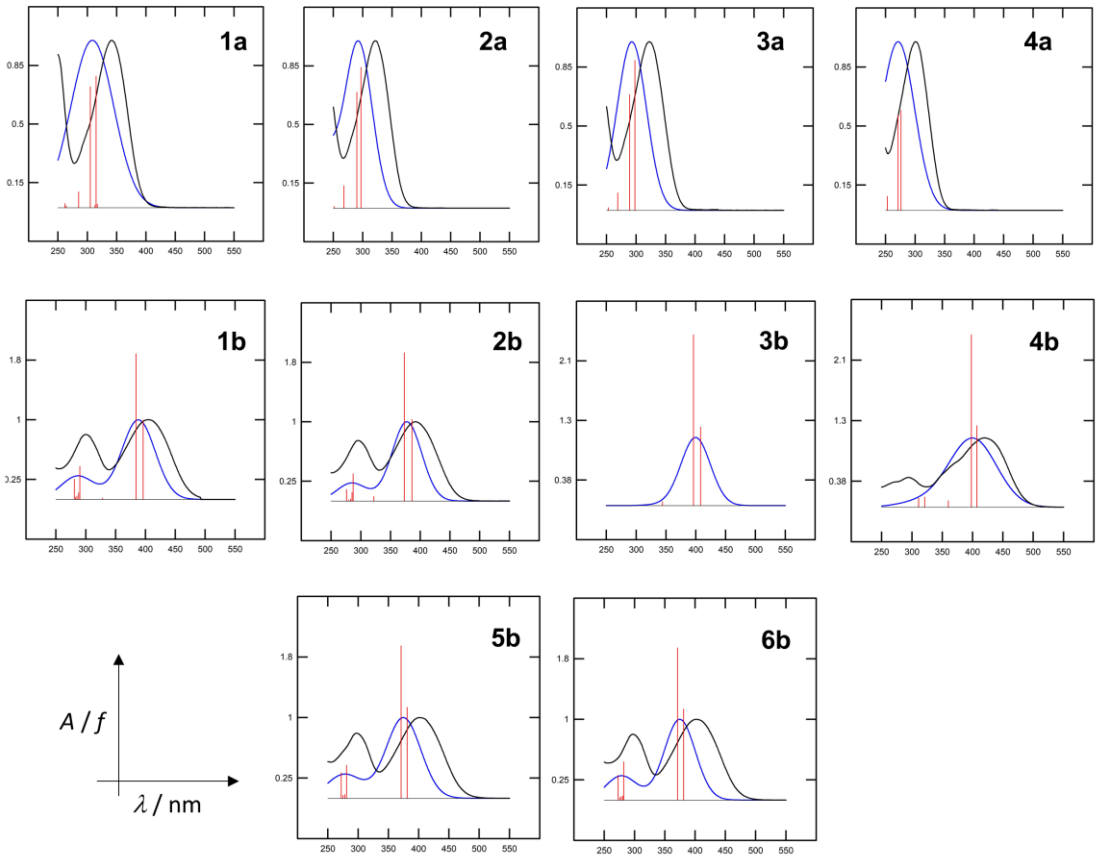

Figure S53. TD-DFT calculated (CAM-B3LYP/6-311+g(2df,p), blue) along with experimental (black) UV-Vis absorption spectra in ACN. The red vertical lines represent oscillator strengths (*f*).

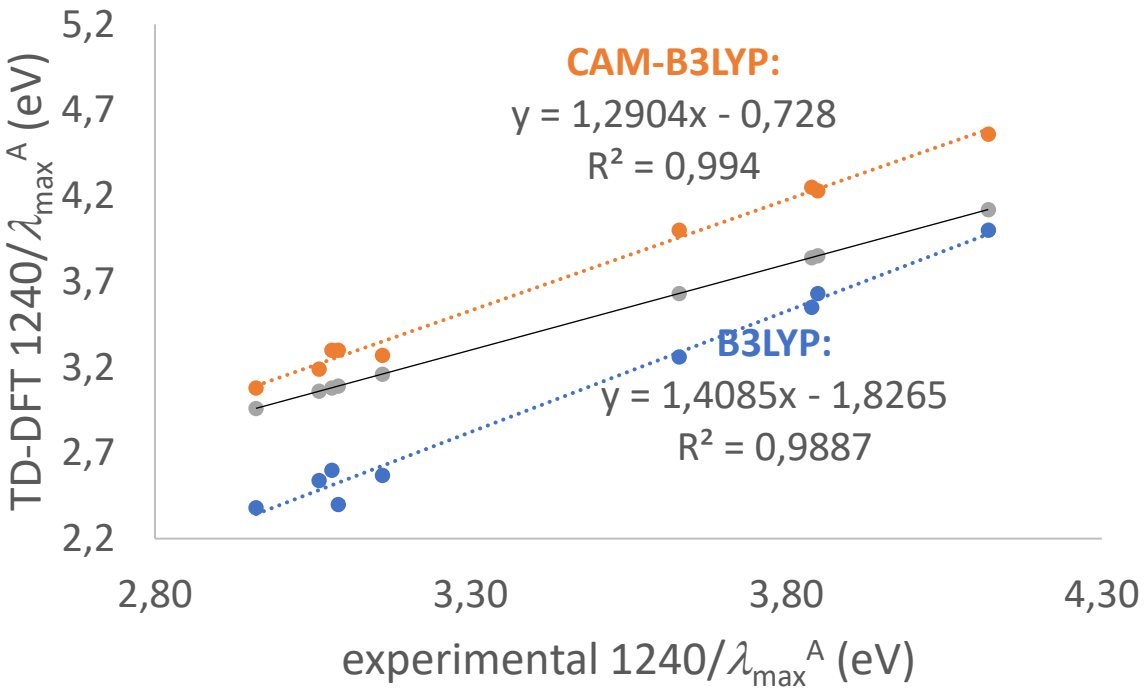

Figure S54. Correlation of the experimental and TD-DFT calculated optical gaps using B3LYP (blue) and CAM-B3LYP (orange) methods. The grey points/line represent experimental optical gaps plotted vs. experimental optical gaps (y = x).